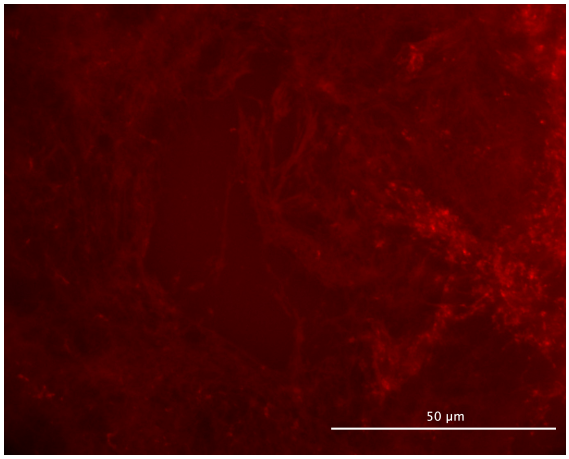

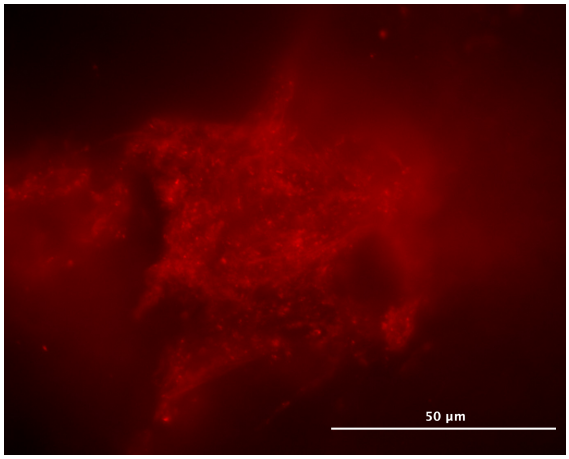

Hydrogels as scaffolds for stem cell therapy with focus on cartilage

Master's thesis in Biotechnology

OLIVER FORSELL

DEPARTMENT OF CHEMISTRY AND CHEMICAL ENGINEERING
APPLIED CHEMISTRY

CHALMERS UNIVERSITY OF TECHNOLOGY
Gothenburg, Sweden 2023
www.chalmers.se

MASTER'S THESIS 2023

Hydrogels as scaffolds for stem cell therapy with focus on cartilage

OLIVER FORSELL

DEPARTMENT OF CHEMISTRY AND CHEMICAL ENGINEERING
APPLIED CHEMISTRY
CHALMERS UNIVERSITY OF TECHNOLOGY
Gothenburg, Sweden 2023

Hydrogels as scaffolds for stem cell therapy with focus on cartilage
OLIVER FORSELL

© OLIVER FORSELL, 2023.

Supervisors: Hanne Evenbratt, Cline Scientific AB & Marina Marinea, Chemistry and Chemical engineering
Examiner: Anna Ström, Chemistry and Chemical engineering

Master's Thesis 2023
Department of Chemistry and Chemical engineering
Division of Applied Chemistry
Chalmers University of Technology
SE-412 96 Göteborg
Sweden
Telephone + 46 (0)31-772 1000

Cover: The picture on the right is a fluorescent images of a collagen network. The picture on the left is a similar network integrated within an alginate hydrogel. See figure 8 (c) on page 23 and figure 31 (c) on page 42 respectively for more information.

Typeset in LaTeX
Gothenburg, Sweden 2023

Abstract

Osteoarthritis, a disease arising from degradation of articular cartilage in joints, presents a major cost for the healthcare system and is a leading reason behind work disability. Conventional therapies are temporary fixes with limited applications and an inability to fully restore the damaged tissue. In recent years, cell therapy has emerged as an alternative and regenerative cartilage therapy. Challenges remain in developing proper scaffolds which serve the purpose of protecting the cells and preventing migration while providing the right mechanical and biochemical signals ensuring high cell viability, proper differentiation and phenotype maintenance. In this study, hydrogel scaffolds were formulated with the objective to achieve both sufficient biochemical and mechanical properties by attempting to create an interpenetrating network (IPN) of polymers forming physical and covalent crosslinks. To determine whether an IPN could be obtained, gels with a variety of crosslinking degrees and polymer concentrations were formulated using a Box-Behnken design of experiments. The gelation kinetics were investigated using a rheometer and molded gels were mechanically tested with a universal testing machine as well as structurally characterized by fluorescent microscopy. A positive synergistic effect was observed with respect to the torsional elasticity but not for unconfined axial compression. Microstructure analysis revealed impact of polymer type and concentration on dispersion quality.

Keywords: Hydrogels, crosslinking, osteoarthritis, cartilage, cell-therapy, rheology, microscopy

Hydrogels as scaffolds for stem cell therapy with focus on cartilage

OLIVER FORSELL

Department of Chemistry and Chemical engineering
Chalmers University of Technology

Acknowledgements

I would like to express my gratitude towards my examiner Anna and my supervisor Hanne, the representative from Cline Scientific. Thank you for all the fruitful discussions, suggestions and ideas during the weekly meetings that enabled me to move in the right direction. I would also like to give a special thanks to my co-supervisor Marina who helped me out immensely in the beginning of my project, providing me with useful tips and tricks for how to conduct the laboratory work and assisted me continuously throughout this project.

Next, I wish to thank Cline Scientific for making this exciting collaboration between the industry and academia possible. Specifically, I wish to thank their employee Reza who provided us with the cells for the experiments throughout the projects.

I also wish to thank everyone at the division of Applied Chemistry in the Department of Chemistry and Chemical Engineering at Chalmers University of Technology who supported me in any way, everything from looking for missing chemicals to instructing me how to use the instruments properly. In particular I would like to thank Mats Hulander for sharing his knowledge on how to operate the fluorescent microscopes.

Finally, I would like to thank myself for embarking on this journey that has been very rewarding but also challenging at times and hopefully prepared me well for the future where new adventures in the field of biomedicine await.

Gothenburg, May, 2023

Glossary

Toughness is defined as the amount of energy a material is capable of absorbing per unit volume before rupture occurs.

The elastic modulus is the stress to strain ratio in the linear viscoelastic region (LVR, the strain region in which a material deforms reversible. Beyond this point the material deforms irreversible, also known as plastic deformation.

Young's modulus, also known as stiffness, is a measure of the elastic modulus during axial compression, characterised by the linear region of the stress-to-strain curve.

Fracture stress is the stress exerted by a specimen prior to rupture.

Storage (G') and loss (G'') modulus are measures of the elastic and viscous modulus respectively during torsional compression, i.e oscillatory measurements such as time and frequency sweeps. Storage modulus is also referred to as shear strength.

$\tan(\delta)$ is equal to the ratio $(G')/(G'')$ and thus a measure of the viscoelastic state during torsional compression. Point of gelation is typically defined as $\tan(\delta) = 1$. $\tan(\delta)$ is also referred to as the viscosity (∇).

Contents

1 Introduction

This section presents a background to the project, which is centred around the lack of a long-term efficient treatment of the degenerative joint disease osteoarthritis. The section starts with a brief description of the disease including the pathophysiology along with its prevalence and various causes. Next, current treatments and presented, focusing on cell therapy and the advantages of encapsulating induced pluripotent stem cells (iPSCs) in a scaffold. Following this, the characteristics of an ideal scaffold are discussed. The section ends by looking at the specific aims of this project.

1.1 Osteoarthritis - causes, prevalence & current treatments

Osteoarthritis (OA) is a widespread issue impacting half a billion people globally [1]. The condition arises from damage of the articular cartilage (AC) tissue in the joints, e.g. caused by trauma or wear and tear, and is becoming more prevalent owing to the ageing population and the increase in obesity [1, 2]. AC normally acts as a smooth and lubricating surface at the end of bones in joints which minimises friction during movement and bears load [3]. The pain and stiffness caused by the damage typically results in physical inactivity making it one of the most common reasons of disability worldwide and a major threat to the health of the individual [1, 2, 4]. More specifically, it is the second most common reason behind inability of working at the age of 50 and older, thereby having a substantial impact on the economy as a whole and the financial situation of the affected individuals in particular [5]. Moreover, it is a major healthcare issue, with the aggregated costs of treatment making it the second most expensive health condition in the US [6].

Damage of the AC is particularly problematic owing to its low repair capacity which is partially attributed to its avascular and aneural nature [7–9]. As a consequence nutrient is only provided by means of diffusion via the synovial fluid, whose production is stimulated by movement, and therefore repair is largely prevented due to the inactive lifestyle typical of the OA sufferer. Moreover, even in the presence of nutrient supplied by the synovial fluid, repair is hampered by the high density of the extracellular matrix (ECM) along with high levels of protease inhibitors which largely prevent movement of the small population of chondrocytes, i.e. the cartilage producing cells, to the damaged area [9, 10].

1.2 Cell therapy - MACI, cell source & loading of the scaffold

Current treatments of AC lesions depend on the injury extent and character, ranging from non-surgical options such as pain-killers/anti-inflammatory drugs and prescription of dietary changes/physical activity to surgical options including marrow stimulation techniques, primarily micro-fracturing. In severe cases arthroplasty is performed, i.e. complete joint replacement, with its associated risk of infections and/or expelling of the protheses. [7, 11, 12]. However, common for all is that they are temporary fixes that are incapable of recreating the original structure of the cartilage [9, 13]. Moreover, in many cases the treatments are less effective for older patients and require a long period of rehabilitation.

In recent years, cell therapy has become a widespread form of treatment, specifically autologous chondrocyte implantation (ACI); for this treatment healthy chondrocytes are harvested from a less load bearing and healthy region of the cartilage, expanded in monolayers and subsequently implanted in the cartilage lesion to regenerate the cartilage. Based on ACI, matrix-assisted chondrocyte implantation (MACI) was later developed in which the cells are encapsulated in a scaffold to prevent migration from the lesion and to maintain their phenotype [11]. The use of autologous cells, i.e. those belonging to the patient, is advantageous because they are easily accessible and do not activate the immune system, however it comes with multiple drawbacks including the limited amounts available, the risk associated with the multiple surgeries and dedifferentiation/phenotypic changes of the chondrocytes during monolayer expansion [7, 11, 14]. Multipotent mesenchymal stem cells (MSCs) present another option by being more resistant to dedifferentiation during expansion and the possibility of using allogeneic cells, i.e. cells obtained from other people [11]. However, several studies show that MSCs are prone to become hypertrophic chondrocytes and therefore creating bone rather than hyaline cartilage. By turning to induced pluripotent stem cells (iPSCs) as a cell source all of the aforementioned shortcomings and risks associated with autologous cells can be avoided. Moreover, consistent proper differentiation into chondrocytes can be achieved by providing suitable concentrations of growth factors. This has been investigated by the company Cline Scientific and resulted in the development of the Cline Nano Gradients, a plate coated with a gradient of growth factors on which the iPSC are grown to identify optimal concentrations for consistent differentiation towards chondrocytes [15]. To finalise and maintain differentiation upon dispersing the cells in a scaffold it is necessary that the chondrocytes are provided in the form of aggregates to ensure sufficient intercellular interactions, providing necessary cues [16].

1.3 Properties of an ideal cell scaffold

In order to utilise the iPSC derived chondrocytes for treatment of cartilage injuries a proper scaffold is desirable. A suitable scaffold acts as protection for the cells and prohibits migration out of the damaged area while simultaneously stimulates propagation and production of ECM, thereby restoring the damaged cartilage [11]. More specifically, a porous structure is required for allowing nutrients to enter via synovial fluid and provide space for cells to grow [17]. Moreover, the scaffold should consist of compatible components including bioactive molecules stimulating cell attachment, proliferation and differentiation [18].

Since the nutrient supply of the cartilage is provided by the synovial fluid which requires movement of the joint to be released into the area, as previously described in section 1.1, the ability of the scaffold to withstand sufficient mechanical forces is a necessity. Moreover, optimising the mechanical properties of the scaffold is particularly important as it has previously been demonstrated that the stiffness and subjection to mechanical loads has a major influence on cell proliferation, migration, adhesion and differentiation [14, 16, 17]. The mechanical properties that an artificial matrix should fulfil includes sufficient strength and modulus, to minimise the stress put on surrounding cartilage [13]. Furthermore, yet another set of important mechanical properties are the time-dependent ones, including creep and stress relaxation to ensure

the gels can withstand loads and strains over extended periods of time. Finally, the deformational-dependent permeability of the scaffold is also of importance for the mechanical strength of the gel since it dictates the load distribution between the solid and fluid phase of the gel [19].

1.4 Aim

The first main objective was to formulate a hydrogel-scaffold that mimics the mechanical and biochemical properties of native cartilage such that, when combined with iPSCs derived chondrocytes, it results in the formation of tissue with the characteristics of articular cartilage. Specifically, this was attempted by introducing collagen into an alginate hydrogel network and perform crosslinking [redacted] respectively in hopes of creating a two-component gel interpenetrating network. The desirable outcome is a synergistic gelation which enhances the mechanical properties of the gel while simultaneously providing the bioactivity of collagen for boosting cartilage regeneration. Several different gel compositions and crosslinking degrees with respect to alginate and collagen were investigated, as both scaffold biomechanical properties and cell-adhesion ligand density have previously been demonstrated to play key roles in controlling stem cell differentiation and ability to produce *de novo* articular cartilage [20, 21]. Another major challenge to resolve was how to achieve proper cell loading into the scaffold, i.e. minimising cell loss without compromising cell viability nor the structural integrity of the scaffold. This was attempted by investigating several different loading and cell dispersion techniques.

2 Theory

The following section covers various aspects to consider when constructing a cell scaffold including the composition and mechanical properties of articular cartilage (AC), the advantages of using alginate-based calcium-crosslinked hydrogels and how to control their gelation rate, as well as the role of collagen in the scaffold and how to stain for it. The section is ended by a brief discussion on the societal, ethical and ecological considerations of the project.

2.1 Composition & mechanical properties of articular cartilage

Native articular cartilage (AC) is comprised of 60-85 % water, 15-22 % collagen fibers and 4-7 % aggrecan and is zonally stratified as illustrated schematically in figure 1 below [13, 22].

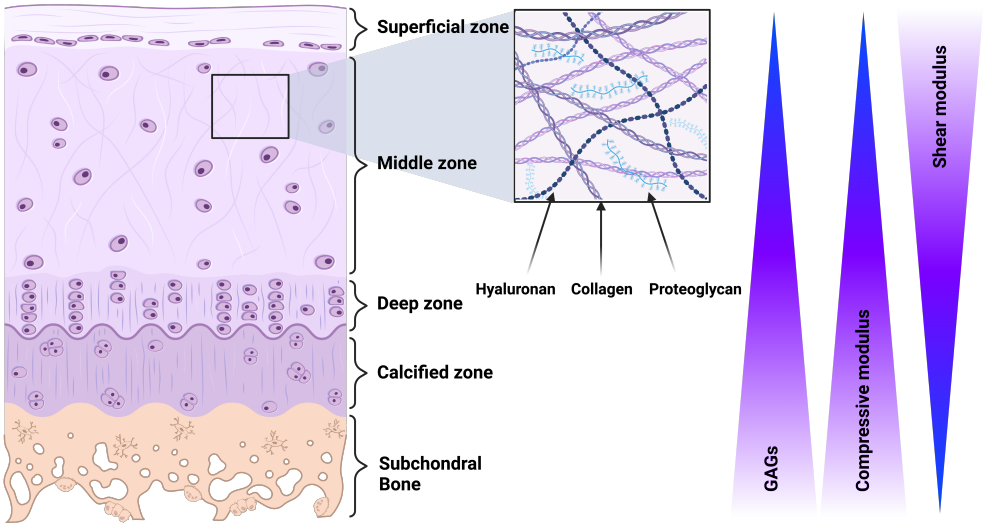

Figure 1: A schematic overview of the zonal stratification of articular cartilage. Created with BioRender.com

The collagen network of the superficial zone is oriented parallel to the articular surface and provides shearing strength as well as resistance against tensile extension, with reported tensile strength and tensile modulus ranges of roughly 10-40 and 50-225 MPa respectively [13, 22]. In the middle and deep zones glycosaminoglycans (GAGs) such as hyaluronan together with proteoglycans (PGs), i.e. GAG-coated proteins such as aggrecan, creates negatively charged aggregates entrapped in the collagen network which in turn results in an osmotic pressure that provides resistance to compressive deformation, with reported compressive strength and compressive (Young's) modulus ranges of roughly 10-60 and 10-20 MPa respectively [13]. The contribution from the osmotic pressure is highlighted by a study which demonstrated up to a 15-fold decreases in compressive strength when comparing the peak and equilibrium stress post relaxation [23]. The tests were carried out in an unconfined setting, allowing secretion of water from the cartilage and thereby drastically reducing the compressive strength. One study conducting unconfined compression trials demonstrated a

compressive modulus of 10 MPa and no statistically significant difference following cyclic loading for 8000 cycles at 4 Hz [24]. However, it should be noted that a study demonstrated that matrices with stiffness as low as 2-100 kPa was enough to stimulate sufficient production of collagen and PGs by chondrocytes in an alginate-gelatin hydrogel [17]. Therefore, it is not necessary to create gels with mechanical properties similar to AC to ensure production of *de novo* cartilage ECM. Moreover, the ECM formed will continuously strengthen the mechanical properties of the hydrogel and therefore make it capable of withstand increasing loads from the patient.

In vivo studies using radiographic techniques such as MRI have demonstrated experienced physiological deformation of the AC ranging between 3 and 7 % immediately post a normal jogging or hopping activity [24]. It should be noted that these reported values fall somewhere in between the true peak strain and the equilibrium strain. The physiological deformation speed of the cartilage was less than 200 ms in a study, as assed by applying an half-body axial load to a patient. Assuming a strain of 5 % and an average cartilage thickness of 2 mm, this would correspond to a strain rate of 0.5 mm/s. However, the strain rate would be much higher in the case of higher loading, e.g. in the case of dropping from a large height. Moreover, the physiological loading frequency experienced during running has been reported to be around 1.2 Hz.

2.2 Alginate hydrogels as cell scaffolds

Hydrogels are a class of scaffolds which are particularly suitable for mimicking AC owing to their capacity to absorb large amounts of liquid, thereby having structural features that mimics those of the cartilage ECM [25]. Moreover, it is easy to incorporate cells and the gel is mouldable, enabling proper fit in the cartilage lesion [26]. A hydrogel is composed of cross-linked polymers that retains a large amount of water. Alginate is an appropriate natural polymer for biomedical use owing to its low cost, low toxicity, high biocompatibility and inert nature [27–29]. For these reasons, alginate has been extensively researched in the past for biomimetic purposes and for use as a cell scaffold in articular cartilage tissue engineering [28].

Moreover, alginate is a shear-thinning biomaterial, i.e. when used for cell injection it reduces flow resistance and the shear stress the cells are subjected to [30]. Furthermore, the mechanical properties of alginate provides cell protection against spikes in extensional forces, which occur particularly at the syringe-needle interface. The protection against shear and extensional forces improve cell-viability post-injection. Alginate can be obtained from brown seaweed and is composed of varying proportions of poly-b-D-mannuronic acid (M) and poly-a-L-guluronic acid (G) [31]. Mild physical gelation occurs upon introduction of divalent cations such as calcium ions creating load bearing junctions by interaction with G-blocks according to the egg-box model as illustrated in figure 2 below.

Calcium ions are preferable to use as crosslinkers compared to other ions due to their low cytotoxicity [28]. The strength of the gel correlates with the amount of calcium ions provided until saturation of the G-blocks is reached [27, 32]. Therefore, the mechanical properties of the gel are highly dependent of the alginate G-content, with higher G/M ratios resulting in stronger and more brittle gels whereas lower ratios

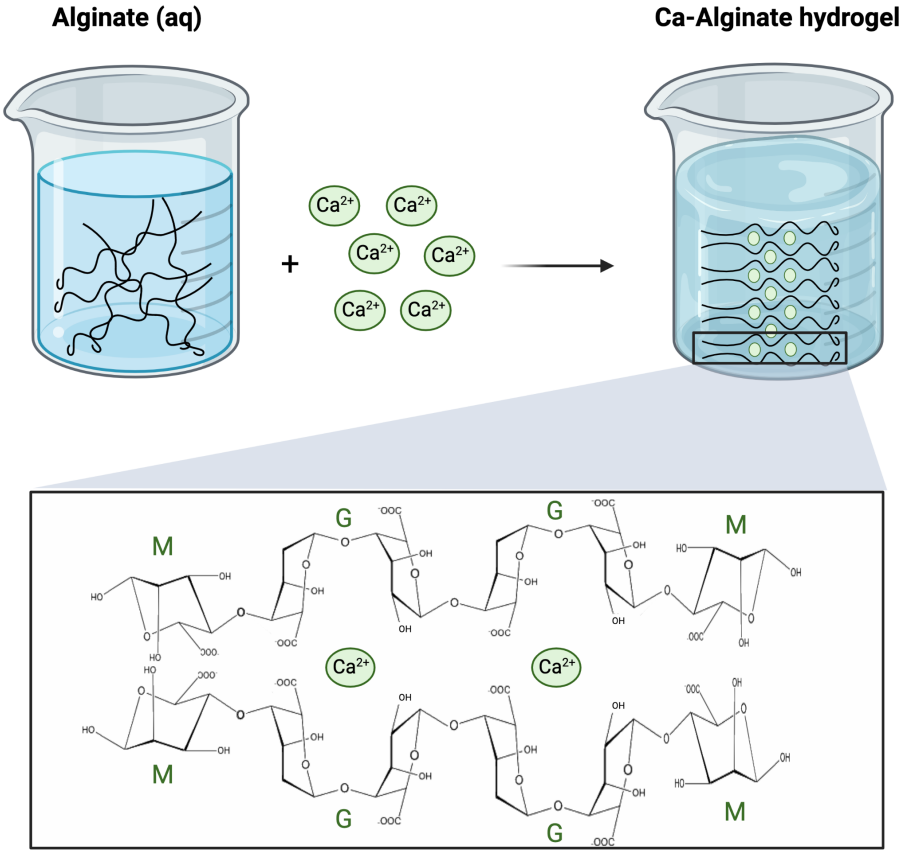

Figure 2: A schematic overview of the egg-box model for alginate gelation by Ca^{2+} ions. Created with BioRender.com

generate weaker and less brittle gels [31]. In addition to the compressive strength, it has previously been demonstrated that the shear strength, as determined by the storage modulus, increases with the calcium crosslinking degree [33]. However, the fracture strain has been reported to be independent of the calcium concentration. A study by Farres et al. demonstrated an instantaneous compressive modulus of roughly 14 kPa for 2 % (w/v) alginate gels saturated with calcium ions having dimensions of 23 mm in diameter and 10 mm in height and being compressed at 1 mm/s.

Additionally, it has been shown that mixing of high molecular weight (MW) alginates with low MW, highly purified, alginate G-block segments can improve gel strength, possibly by means of acting like a glue between topologically restricted polymers [34]. The polydispersity index (PI) is a measure of the MW distribution of an alginate product with a PI > 2 being a relatively wide distribution which indicates that different batches of alginates has been mixed together or alternatively that degradation is occurring. Additionally, the gels mechanical characteristics are also a product of the MW of the alginate monomers with gel strength reported to correlate with MW at least until 300 kDa. Finally, it has been demonstrated in a study by Mooney *et al.* that the viscoelastic properties of an alginate matrix, as influenced by alginate MW and measured by stress relaxation times, does play a role in dictating tissue organisa-

tion and morphogenesis [35, 36]. For alginate gels with a MW of 138 kDa the reported stress relaxation half times were roughly 350 $\pm 100s$.

2.3 Retardation of the alginate gelation

Gelation of alginate occurs irrespective of the temperature, a rare feature known as cold setting [34]. The gelation kinetics on the other hand are influenced by the temperature at which the gelation occurs as well as the resulting gel strength. Moreover, owing to the polyelectrolyte nature of the alginate, its interaction with other charged polymers in a mixed system, including proteins, have been reported to influence e.g. the viscosity and Young's modulus of the gel. The influence on the viscoelastic and mechanical properties are therefore highly dependent on the pH and ionic strength of the environment. However, to exercise more controlled retardation of the alginate gelation other methods are applied. In the case of ionic crosslinking, an ion such as calcium can be complexed with a chelating agent, such as EDTA or citrate, or it can be provided in the form of a salt such as $CaSO_4$ or $CaCO_3$ with poor solubility in neutral aqueous solutions, a set of methods referred to as internal setting. A change of pH induces a slow and gradual release of calcium ions (Ca^{2+}). By ensuring a gradual release of Ca^{2+} potential issues associated with rapid network formation are avoided, particularly precipitation of polymers prior to homogenous dispersion of Ca^{2+} in the solution such as in the case of using diffusion setting like $CaCl_2$ [37]. Moreover, a major advantage of such an injectable system is the possibility of immediate integration of the newly formed ECM with the surrounding tissue, a feature that is particularly advantageous for articular cartilage replacement since artificial cartilage produced *ex vivo* might not adhere with the surrounding tissue of a damaged area [16, 38]. Several conventional matrices, including polyglycolic acid (PGA) based ones, lack this attribute and remain unstable for several weeks following cell seeding. Additionally, an injectable gel system eliminates the need of moulding the damaged area and subsequently implanting the construct, therefore being a much less invasive option.

A change in pH can e.g. by achieved by introducing glucono-δ-lactone (GDL). The GDL is deprotonised upon introduction in the aqueous solution, a method which as previously been employed extensively [27]. In the case of using $CaCO_3$, adding GDL in stochiometric equivalent amounts ensures the pH of the solution remains unchanged throughout the gelation process according to the following reactions [37].

$$CaCO_3 + 2H^+ \rightarrow Ca^{2+} + H_2CO_3 \tag{1a}$$

$$H_2CO_3 \rightarrow H_2O + CO_2 \tag{1b}$$

This is a desirable feature of the gelling components since the ionisation of alginate, and therefore the capacity to crosslink with Ca^{2+}, is pH-dependent but most importantly because cells, which require a pH similiar to *in-vivo* conditions, will ultimately be introduced into the gel. The drawbacks with this method is the evolution of $CO_{2(g)}$ and $H_2O_{(l)}$ which impacts the mechanical properties of the hydrogel created [39]. Another internal gelling method with stable pH throughout the gelation process is the

Competitive Ligand EXchange crosslinking (CLEX) crosslinking system established by Yamamoto *et al*, of which an example is illustrated in figure 3 below.

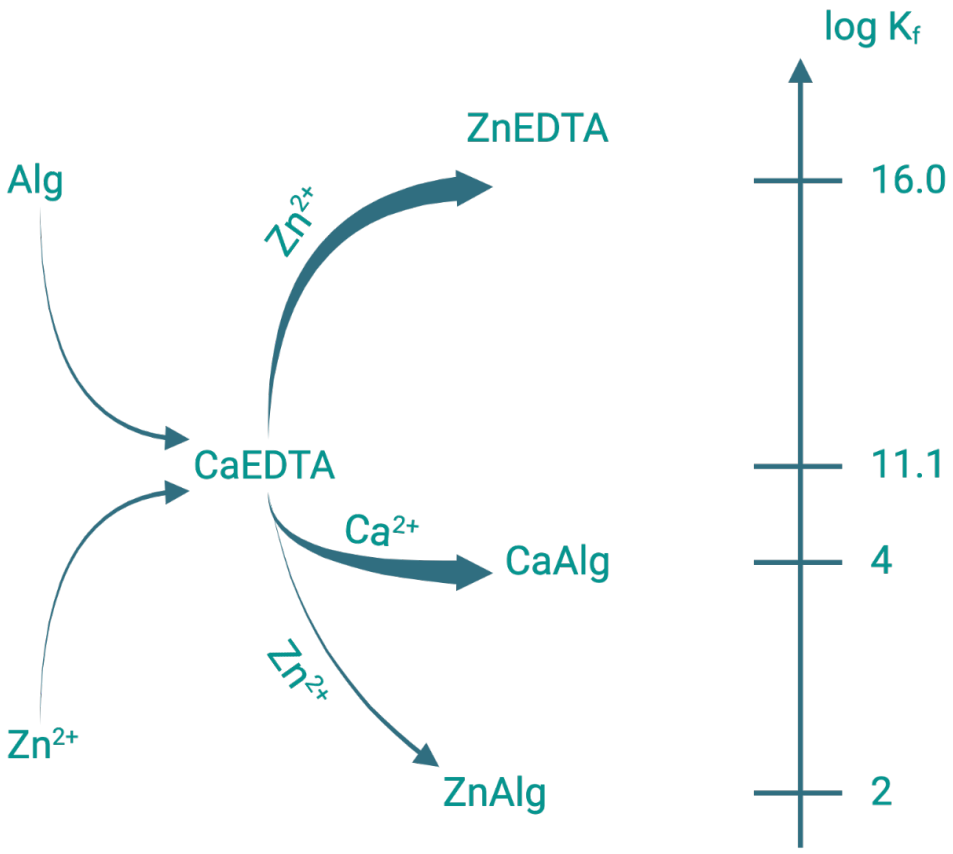

Figure 3: A schematic overview of an example of the CLEX crosslinking system. Created with BioRender.com and adapted from figure 1 in [39]

The CLEX system utilises the difference in affinity of two multivalent ions to alginate and two chelators, one of them e.g. being EDTA as in figure 3 above [39]. The multivalent ions consist of a crosslinking ion (CI), such as Ca^{2+}, and an exchange ion (EI), such as Zn^{2+}. Two alginate solutions are prepared; one containing the CI and a chelator with higher affinity to the CI than alginate, the other one containing the EI and a chelator with higher affinity to the EI than alginate but lower towards the CI when compared with alginate. Importantly, the EI has a higher affinity towards the CI chelator than the CI and therefore, upon mixing of the solutions, CI is substituted for the EI at the CI chelator and the CI is able to crosslink with the alginate. By changing the chelators involved the kinetics of the process can be altered.

Additionally, phosphate can be provided which acts a a chelator of calcium, i.e. reducing the available calcium for the alginate monomers, thereby slowing down the gelation rate [28]. This results in more uniformity as well as improved mechanical properties due to the greater order of the cross-linked network that is achieved with slower gelation rates [28, 40]. Once implanted *in-vivo*, the gel will gradually dissolve owing to the ion exchange with the surrounding fluid replacing the calcium ions with monovalent

ions, calcium chelators and non-crosslinking divalent ions, thereby making room for production of ECM and successive cartilage regeneration by the chondrocytes [41]. Studies have been made *in vitro* showing the feasibility of adjusting the concentration of ions in the culture medium to tweak the degradation rate of calcium crosslinked alginate hydrogels. Moreover, the mixing of alginates with different MWs and oxidisation states has been successfully implemented to control degradation rate and introduce porogens, i.e. pore-forming components, into the scaffold to provide space for cell growth and ECM production [42]. Ideally, a major degradation of the scaffold has occurred within the first month of implantation as this is a crucial time period for formation of new cartilage tissue [29].

2.4 Collagen - cell adhesion, structure, fibrillogenesis & sources

A hydrogel composed of non-modified alginate alone does not provide a sufficient environment for cells to thrive, as the lack of proper binding sites causes cell aggregation and potentially dedifferentiation [14, 28, 43]. To resolve this issue an additional component is required and a suitable candidate is collagen, the most abundant component in natural articular cartilage [44]. Moreover, combining collagen with an alginate hydrogel is particularly suitable as the latter does not mask the cell-adhesion sites provided by the collagen [45]. Noticeably, it has already been demonstrated that gels with an interpenetrating network (IPN) of alginate and collagen is possible to formulate, defined henceforth as completely intercalated networks throughout the gel, and allows for independent control of the stiffness/storage modulus by regulating the alginate crosslinking degree [46]. When conducting frequency sweeps, a weak power function relationship between the storage modulus and the frequencies has been observed. The incorporation of collagen in an alginate hydrogel stimulates chondrocyte attachment, proliferation and production of cartilage specific ECM [9, 26, 28]. The collagen induces cell activity by interacting with the cells via adhesion sites [47]. Specifically, it is thought that the interaction between cells and collagen at collagen adhesion sites is made possible by its Arg-Gly-Asp (RGD) tripeptide motifs, which serve as cell integrins receptor ligands, along with its fibrous structure with characteristic nano-topography. The importance of the nano-topography, a feature which is lacking in most electrospun synthetic nanofibers, is further strengthened by the fact that RGD functionalisation of alginate hydrogels alone has been observed to be insufficient for stimulating chondrogenic differentiation and ECM production [48]. In contrast, it has been demonstrated that collagen incorporation in alginate hydrogels enables maintenance of the differentiated stage of stem cell derived chondrocytes [18]. Additionally, cells are even capable of registering the mechanical properties of collagen fibrils, with a study by Xie *et al.* demonstrating that higher fibre stiffness as well as shorter fibre lengths is associated with suppression of cell proliferation and migration by preventing cells from recruiting fibres in the surroundings [49].

The formation of the collagen fibrillar network, fibrillogenesis, is an entirely entropy-driven process *in-vitro* [50]. The stability within each fibril is primarily upheld by intermolecular covalent bonds between residues of individual collagen molecules. Optimal collagen networks, with respect to mechanical strength, are achieved at 37 ° C. Lower temperatures have been associated with poorer mechanical properties, mainly

attributed to the decrease in branching or, equivalently, cross-linking between the collagen fibrils [51]. Moreover, lower temperatures also influence fibre topography creating less compact and short fibres as well as increase fibre stiffness, which has negative influence on cell behaviour as explained in the previous paragraph [49].

A schematic overview of the structure of collagen fibrils and the collagen molecule is presented in figure 4 below.

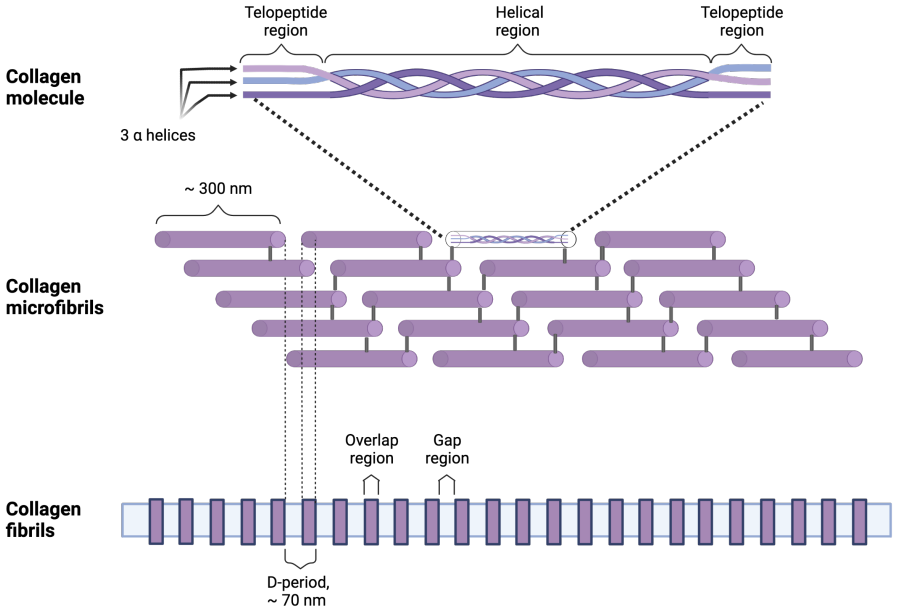

Figure 4: A schematic overview of d-periodic structure of collagen fibrils. Created with BioRender.com

The collagen molecule is composed of three alpha-polypeptide chains [50]. The vast majority of the molecules form a triple-helical structure due to a characteristic Gly-Xaa-Yaa primary structure [53]. Most of the collagens (>90 %) is part of the fibril-forming collagen group which provide torsional stability and tensile strength to a tissue [50]. On each end of the fibrillar collagens there is a nonhelical, telopeptide region which play an important role in the covalent crosslinking of the collagen monomers, i.e. the fibrillogenesis. Each fibril in turn is composed of collagen molecules in a crystalline structure with a D-spacing of approximately 70 nm owing to the roughly 300 nm length of the collagen molecule [50]. This arrangement of the collagen fibrils is known as the Hodge-Petruska-scheme, named after its discoverers, and gives rise to its characteristic macrostructure visible in electron microscope as schematically represented by the the rod-like shape with grooves and ridges in the bottom part of figure 4 above.

The use of recombinant collagen produced using a cell factory has proven successful, but is currently limited by difficulties of scaling and high cost [26]. Therefore, animal derived collagen has been used in this study. However, it should be noted that there is quite extensive product-to-product and batch-to-batch variability for animal-derived

collagen, with physiological condition and age impacting the degree of crosslinking, thereby making comparative studies difficult *in-vivo*[54, 55]. Specifically, collagen preparation methods has a major impact on the quality of the final product, with partial loss of the telopeptides of collagen-molecules negatively impacting fibrillogenesis. Specifically, the use of pepsin or pronase enzymatic digestion has been reported to cause partial telo-peptide loss.

2.5 Fluorescent staining

Eosin B is a fluorescent dye with its anionic carboxylic and phenolic groups having a high affinity towards specific amino acid residues including the polar AAs arginine and lysine at neutral pH, which are common AAs found within the collagen molecule [56, 57]. Immunostaining presents an alternative but it is expensive due to the difficulties of making antibodies specific for collagen subtypes due to the gly-x-y repeat secondary structure [58]

An calcein-AM and ethidium homodimer-1 (EthD-1) assay can be used to perform live/dead imaging of cells [59]. Calcein-AM passes through the cell membrane due to its lipophilic nature and is subsequently metabolized to calcein by esterases The calcein emits a green fluorescence signal in the viable cells. EthD-1 is only capable of entering cells with a compromised cell membrane upon which it binds to the DNA of the nuclues, emitting a red fluorescence signal.

2.6 Societal, ethical and ecological considerations

As previously mentioned, alginate is a derivate obtained from brown algae which has alternative areas of use including as a food resource and, in its natural state, for fixation of carbon. Algae is a renewable product with a low carbon footprint. However, the extraction process for sodium alginate from algae does have a substantial climate impact [60]. Despite this, given that plentiful is available to use, the valorisation when used as a component in regenerative biomedicine and the small volumes required it is safe to claim that the benefits outweighs the drawbacks.

In this specific project collagen was derived from animal sources. Until recombinant collagen production cell factories becomes readily available, as discussed in section 4.8, this is a cost-effective alternative that, due to being a by-product from the meat industry, does not harm animals *per sē*. In clinical applications the use of human collagen would be necessary to reduce the risk of implant rejection and in such a case written consent would be acquired from the donor.

The specific use of iPSCs is more ethically justified than other pluripotent stem cells, such as embryonic stem cells which requires sacrifice of an embryo to be obtained, since they can be derived from a small number of somatic cells and were obtained in a non-invasive manner with written consent [11]. For stem cells containing products in general it is of vital importance that safety measures are in place to ensure no stem cells are present once provided to the patient to ensure no teratomas form in the body. Prior to clinical trials, in vitro, ex vivo as well as in vivo studies in animal models will be conducted to verify that no stem cells are present in the final product.

Animal trials are for natural reasons of ethical concern and should therefore only be performed when no other options are available. For a utilitarian point of view, an ethical view typically adopted in modern science research, the ends should justify the means given the potential hundreds of millions of people who could benefit from an effective treatment of osteoarthritis.

3 Methodology

In the following section the materials and methods used throughout this project are presented. The section starts by presenting a list of the chemicals, consumables and tools used. Following this, the formulation of the gels along with the method of formation is presented. Next, the mechanical tests used to characterise the gels are described, including large and small deformation, followed by the swelling trials. Thereafter, the fluorescence microscopy methods used to visualise the microstructure of the gels and the viability of the cells are presented. Finally, an overview is provided of the statistical analysis performed to investigate the results.

3.1 Materials

A list of the chemicals used throughout the project are presented below.

- MilliQ water
- NaOH
- Acetic Acid
- Manugel DMB (alginate) - FMC, USA
- Gibco^{TM} DMEM/F-12, HEPES, no phenol red - Fisher Scientific, USA
- [redacted]
- [redacted]
- [redacted]
- [redacted]
- Collagen [redacted]
- [redacted]
- LIVE/DEAD^{TM} Viability/Cytotoxicity Kit, for mammalian cells - L3224, Thermofisher Scientific, USA

A list of consumables and tools used are found below.

- Heat plate with magnetic stirrer
- Magnets
- Beaker
- Vials
- Eppendorf tubes
- Pipettes

- Syringes (1,2 x 40 mm)
- pH papers
- Gel molds in plexiglass with 5x5 mm wells (Made in-house)

3.2 Gel formulation

A set of stock solutions was prepared. The alginate source used throughout the project is Manugel DMB (FMC, USA) with a measured MW of 172.4 kDa and a dispersity of 1.381 (Mw/Mn), see appendix A for the complete data obtained by size exclusion chromatography. A Dulbecco's Modified Eagle Medium (DMEM) (Sigma-Aldrich, USA) stock solution with [redacted] weight percent (wt%) alginate was made by sequentially adding the alginate powder to the DMEM solution while being stirred with a magnetic stirrer at room temperature (RT), each time vigorously shaking the bottle to break up larger particles. Once all alginate powder was added the stirring continued until the alginate was completely dispersed and air bubbles had dissipated. A collagen [redacted] mother solution (MS) was prepared by solubilising the collagen powder in [redacted] acetic acid (AcOH) to a concentration of [redacted] mg/ml in an Eppendorf tube and placing it in the fridge overnight. The solution was subsequently stirred and lightly vortexed to ensure complete homogenisation before being utilised further. The [redacted] was dissolved in MilliQ water to a stock concentration of [redacted], placed in aliquots and stored at -20 °C to avoid repeated freeze and thaw cycles.

To formulate a gel, a [redacted] weight ratio of [redacted] wt % alginate in DMEM and pure DMEM solution respectively was weighed in separate tubes. Since the high viscosity of the collagen MS prevents transfer of the solution with volumetric accuracy, the solution was instead transferred using a syringe from the MS to a separate, pre-weighed, Eppendorf tube, and the volume was calculated by measuring the weight. Importantly, the threshold volume is based on a final solution composed of a [redacted] volumetric ratio of collagen to alginate solution, such that a final concentration of [redacted] wt % alginate is reached for all gels. Based on the obtained volume of collagen the amount of [redacted], deionized water, NaOH and alginate solution to be added to reach the desired final composition was subsequently calculated. Thereafter the compounds inducing alginate gelation, [redacted], were weighed together in a third tube.

The following steps were then performed rapidly to limit the possibilities of fibrillogenesis occurring pre mixing with the alginate solution. First, the pH of the collagen solution was adjusted to between 6 and 7 by addition of 1 M NaOH while on ice. Closely thereafter the calculated amount of [redacted] was added followed by deionized water to reach the desired concentration of collagen and gently mixed by vortexing. Following this the pre-weighed DMEM solution was added to the tube with [redacted] and quickly mixed with a spoon until no undissolved particles were visible, upon which the solution was transferred to the pre-weighed [redacted]

wt % alginate (DMEM) solution. Then, the solution was mixed by vortexing and subsequently transferred in batches using a syringe to the pH adjusted collagen-[redacted] solution placed in a stand on a scale to ensure as close to a correct volume being transferred. The final mixture was then rapidly vortexed before transfer to gel molds once again using a syringe to gel overnight in an incubator at 37 °C or directly placed in a rheometer.

The originally suggested experimental design was revised to conform with the limitations set by the method developed, which is dictated by the solubility of collagen in the MS due to the difficulties of working with higher concentrations of the alginate stock solution. A design of experiments (DoE) was constructed to explore the gel formulations using a response surface methodology (RSM) to establish compositions, i.e. a set of formulation parameter values, with improved mechanical properties, i.e. the response. A Box-Behnken design (BBD) was specifically selected as the DoE to be able to construct a quadratic regression model to fit the response surface, investigating the influence of the different formulation parameters as well as potential interaction and quadratic effects [61]. The BBD requires less experimental runs and is considered more powerful compared to other established DoEs such as central composite design and three-level full factorial design [62, 63].

3.3 Small deformation

A Discovery HR-3 rheometer (TA instruments, USA) equipped with a 40 mm sand-blasted parallel plate geometry (Serial no. 111023) was used to conduct time-sweeps of 100 microliter gel solutions at 0.5 % strain with the single point frequency of 1 Hz to assess the viscoelastic properties and gelation kinetics, what is known as small deformation rheology. This was followed by frequency-sweeps between 0.01 and 60.0 Hz with 5 points per decade. A Peltier plate ensured 37 °C was maintained throughout the runs.

3.4 Large deformation - Unconfined compression

An universal testing machine (Instron, USA) was used to determine the strain to stress relations and the breaking strengths and strains, what is known as large deformation. Gels of 5x5 mm were prepared in molds and incubated at 37 °C overnight. The specimens were tested in an unconfined setting using parallel plates at RT. The speed of the crosshead, i.e. the rate of compression of the specimens, was 2.5 mm/s unless stated otherwise. The rate was chosen to mimic what could possibly be experienced in vivo during heavy loading of the knees.

It should be noted that in this unconfined compression the engineering stress has been calculated which deviates from the true stress since the cross sectional area increases as the specimen is deformed. However, since the gels are assumed to deform in a similar manner with respect to their geometry, the engineering stress is a sufficient relative measurement to explore the difference between the gel formulations with respective to their large deformation properties. Moreover, the height of specimens was defined based on the gap registered at an axial-force of 5 mN to accommodate for

height variations and uneven surfaces of the specimens. When estimating the Young's modulus and the maximum compressive elastic strain, the cut-off was selected as the point at which the correlation of the linear regression was decreasing. For all cases the fit, as determined by the R^2 value, was > 0.99.

3.5 Large deformation - Stress relaxation

Stress relaxation tests were conducted in the rheometer on gels manufactured like those of the unconfined compression trials to assess the intrinsic compressive strength of the solid phase of the gels, i.e. without the influence of the aqueous environment as assessed by unconfined compression. The tests consisted of alternating axial compression at roughly 14 % increment in strain degree in one second per round, with 4 minutes of oscillatory time sweeps at 1 Hz and 0.2 % strain in between each round of compression. Only four compression levels were tested for each specimen to prevent dehydration of the gels prior to the end of the trial. The oscillatory rheology was done within the LVR. The stress relaxation half time t_m is defined as the time point at which the stress is reduced to half of the maximum stress registered.

3.6 Swelling trials

5x5 mm gels were submersed in 1 ml of DMEM nutrient solution at 37 °C that was exchanged 3 times during one week, at which times the mass and volumetric change of the specimens was recorded.

3.7 Fluorescent microscopy of collagen network

A thin slice was cut from 5x5 mm gels and submersed in 1 % Eosin B (Thermo Scientific Chemicals, USA) in DMEM.

The slice was subsequently transferred to a glass slide with a concave cavity. 10 microliters of DMEM was placed around the recess and a 22x22 mm coverglass was placed on top. Fluorescent images of the gel slices were captured using a Zeiss microscope with a HBO lamp and a 100 x objective oil immersion lens with 100x magnification.

3.8 Live/dead imaging of cells

Live/dead staining of the cells was achieved using a calcein-AM and ethidium homodimer-1 protocol (L3224, Thermofisher Scientific, USA).

3.9 Statistics

ANOVA and regression analysis of the data was performed using Minitab®. A significance level of 0.05 was set for all tests. t-tests were carried out for simple comparisons of two sets of data. ANOVA with Tukey's post hoc test was performed for comparisons of multiple pairs of data to control the family-wise error rate, i.e. to reduce the risk of obtaining false positives compared to a simple t-test. It should be noted that this

method instead increase the risk of presenting false negatives due to the requirement of having a much lower α-value for each individual comparison compared to a t-test.

4 Results

In the following section the results from the mechanical and structural investigation of the hydrogels are presented along with results from cell loading trials. The initial parts focuses on the properties of the separate gel systems, i.e. the pure collagen and alginate gels, including the impact of varying the calcium crosslinking degree and how the gelation kinetics can be influenced. The next segment focuses on the combine alginate-collagen gels with fast gelation of the alginate, including their gelation kinetics, large deformation tests, microstructure analysis and the results from cell loading trials. The final part covers combined alginate-collagen gels with slow gelation of the alginate, including a complete Box-Behnken design of experiments to characterise the mechanical properties by large deformation and stress relaxation, microstructure analysis as well as results from cell loading trials.

4.1 Unconfined compression of alginate gels - impact of crosslinking degree

The impact of increasing the Ca^{2+} concentration on the breaking strength of alginate (DMEM) gels is demonstrated in figure 5 below.

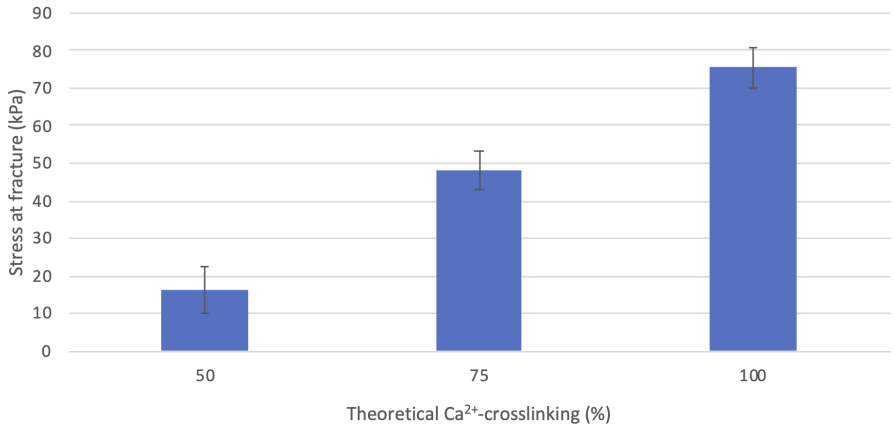

Figure 5: Stress at break for calcium induced 5x5 mm alginate gels at different Ca^{2+} crosslinking degree, measured at crossheadspeed of 1.0 mm/s

As expected, the stress at break of the alginate gels is increasing statistically significantly until 100 % theoretical crosslinking (ANOVA, Tukey's *post-hoc* test). The impact of increasing the Ca^{2+} concentration beyond 100 % theoretical crosslinking on the breaking strength of alginate gels is demonstrated in figure 6 below.

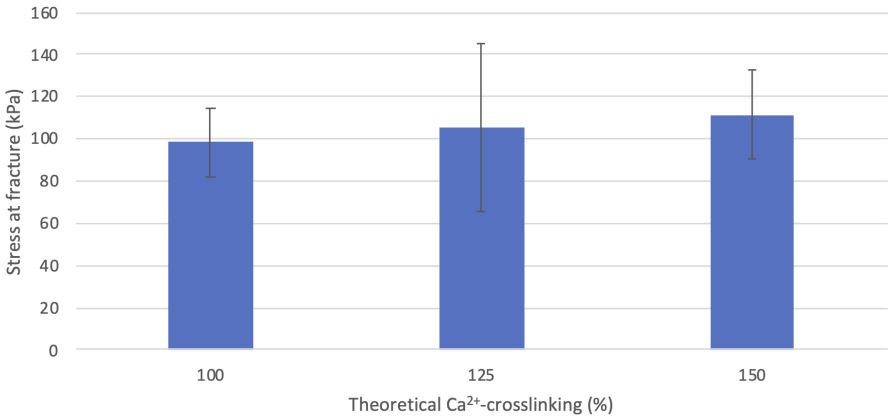

Figure 6: Stress at break for calcium induced 5x5 mm alginate gels at different Ca^{2+} crosslinking degree, measured at crossheadspeed of 2.5 mm/s

In accordance with theoretical calculations, no increase in stress at break is observed for Ca^{2+} concentrations above 100 % theoretical crosslinking (ANOVA, Tukey's *post-hoc* test), since these should have saturated G-blocks and therefore maximum strength achievable as discussed in section 2.2 . Based on the results from the stress at break of alginate gels with theoretical crosslinking >100 %, it appears that the chelating effects from the DMEM nutrient solution as discussed in section 2.3 is rather small. Otherwise, the over-saturation of gels with Ca^{2+} would have been associated with an increased stress at fracture which is not the case already at 125 % theoretical crosslinking. It is noteworthy that the compression rate has a significant impact on the stress at break for the alginate gels, when comparing the 100 % alg gels between figures 5 and 6, which is expected as the network requires time to rearrange properly during compression.

4.2 Collagen solutions - Gelation kinetics and fluorescent imaging

In figure 7 the resulting storage modulus and loss modulus during time-sweep measurements of pure collagen gels with varying [redacted] are compiled.

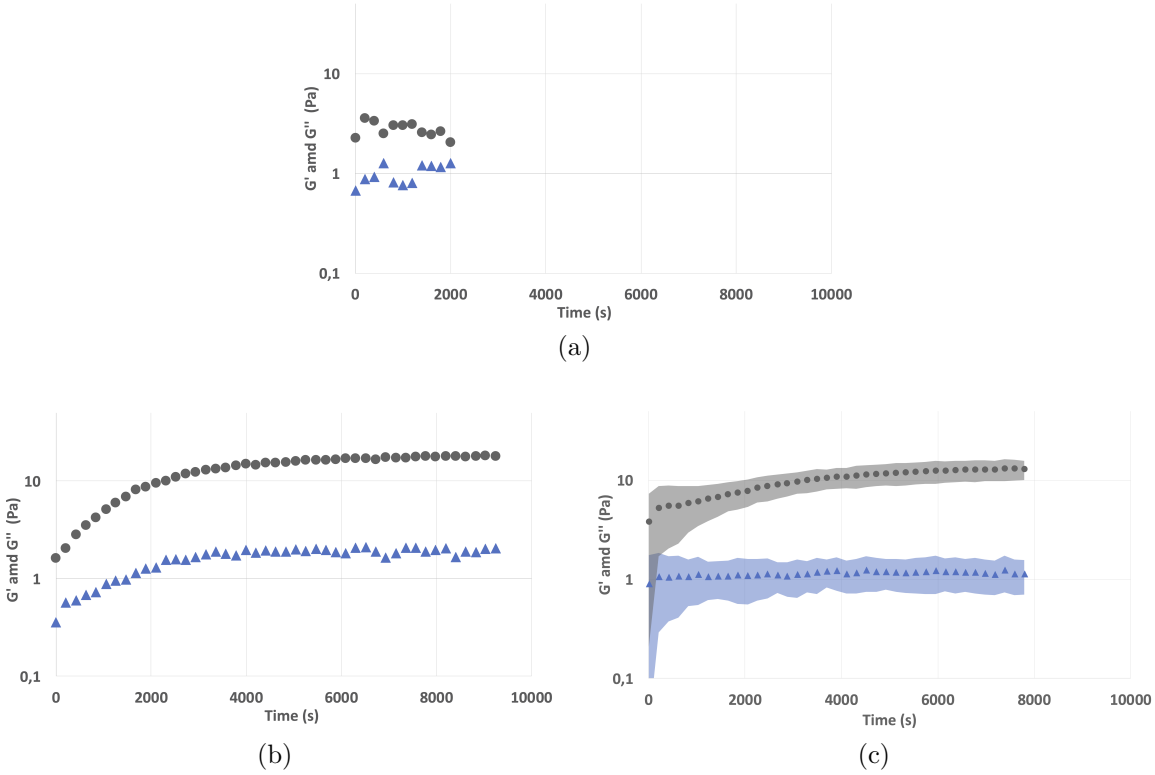

Figure 7: Storage modulus comparison of pure col-gels during time-sweep rheology experiments: (a) Col-[redacted]; (b) Col-[redacted]; (c) Col-[redacted]. Grey dots and light blue triangles symbolise the storage modulus and the loss modulus respectively. The coloured area around the datapoints represents the standard deviation of the modulus.

As evident from figure 7a, collagen did not provide a measurable level of gelation at [redacted] mg/ml without the assistance of [redacted] although $\tan(\delta) > 1$ as indicated by a steady decrease in the viscosity for more than 30 minutes. In contrast, at an [redacted] a noticeable gelation occurs with a final measured $\tan(\delta) < 0.1$. Noticeably, an increase in the [redacted] increase the rate of gelation as evident when comparing figure 7b and 7c. Interestingly, it did not result in a significant increase in the final G' achieved, indicating that the optimal [redacted] should lie somewhere in this range. This is in contrast to what has previously been reported in a study by [redacted], indicating that greater torsional strength should be possible at [redacted] and could be attributed to the [redacted]. The registered storage modulus is very low in all cases when compared to a previous study by [redacted], although the difference can at least partially be attributed to a smaller gel volume being used. It is possible that the remaining difference is largely a result of the lower collagen concentration.

Figure 8 contains fluorescent images captured of collagen solutions with varying concentration and [redacted].

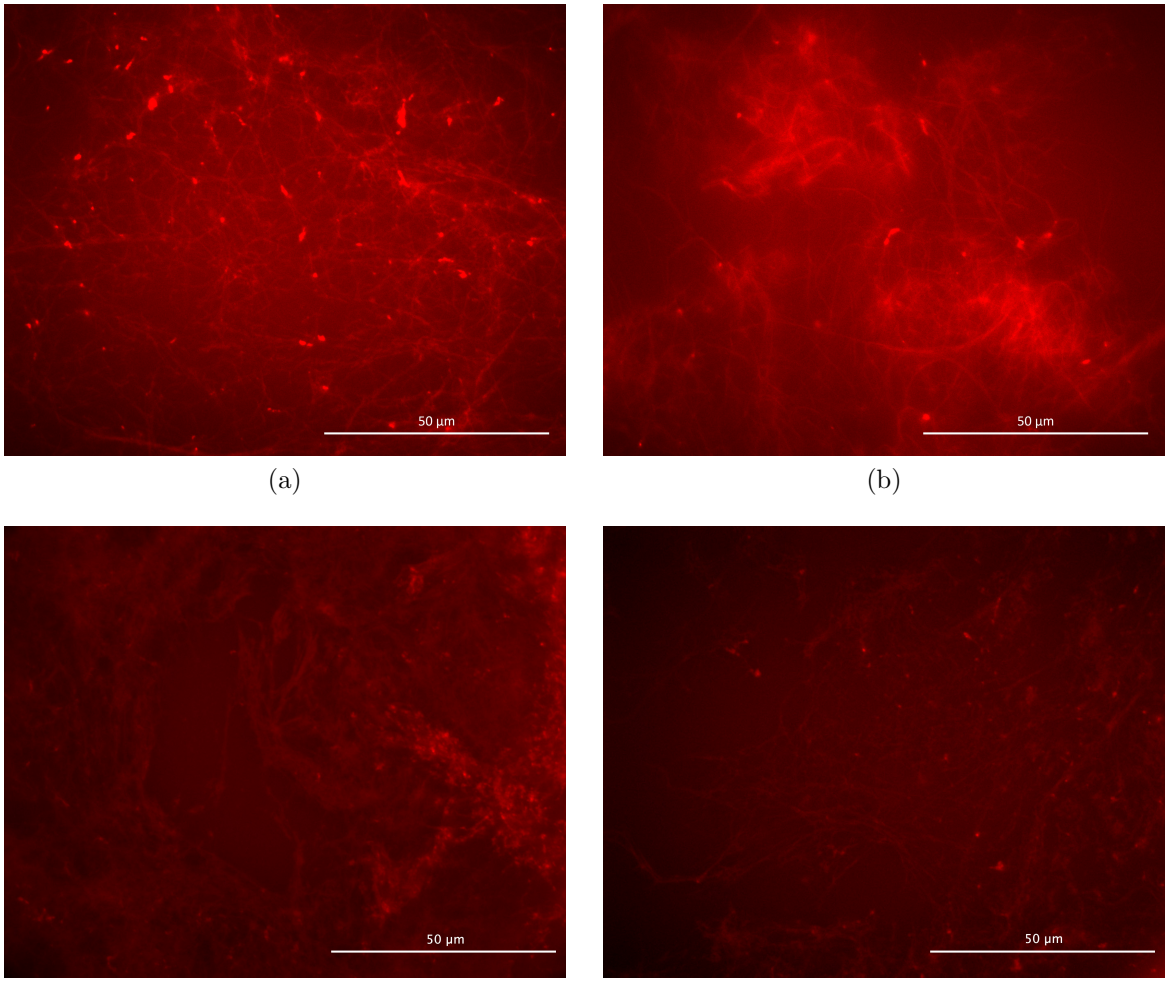

(a) (b)

(c) (d)

Figure 8: Collagen gels incubated at 37 °C stained red with 1% Eosin Band imaged with a 100x magnification oil immersion lense. (a) Col-[redacted]; (b) Col-[redacted]; (c) Col-[redacted]; and, (d) Col-[redacted]

The individual collagen fibres composing the network are clearly visible as indicated by the red strands, in particular for the solutions without [redacted]. With increasing collagen concentration more clustered areas of collagen are observed as evident from figure 8a. The clustering of collagen was even more pronounced in the samples containing [redacted] as evident when comparing figure 8b with figure 8 (c) and (d). As expected, the topography of the fibres appears visually similar to collagen fibres incubated at 37 °C when compared to lower temperatures in a study by Xie et al as discussed in section 4.8. The network appears more porous which is also expected given the lower concentration. For all cases, the collagen network was not evenly dispersed and only covered a fraction of the sample area with an unfilled space particularly evident in figure 8c.

4.3 Gelation kinetics is controlled by varying the Ca^{++} source

A comparison of the gelation kinetics when varying the Ca^{++} source compared to a col-[redacted]-gel is shown in figure 9 below.

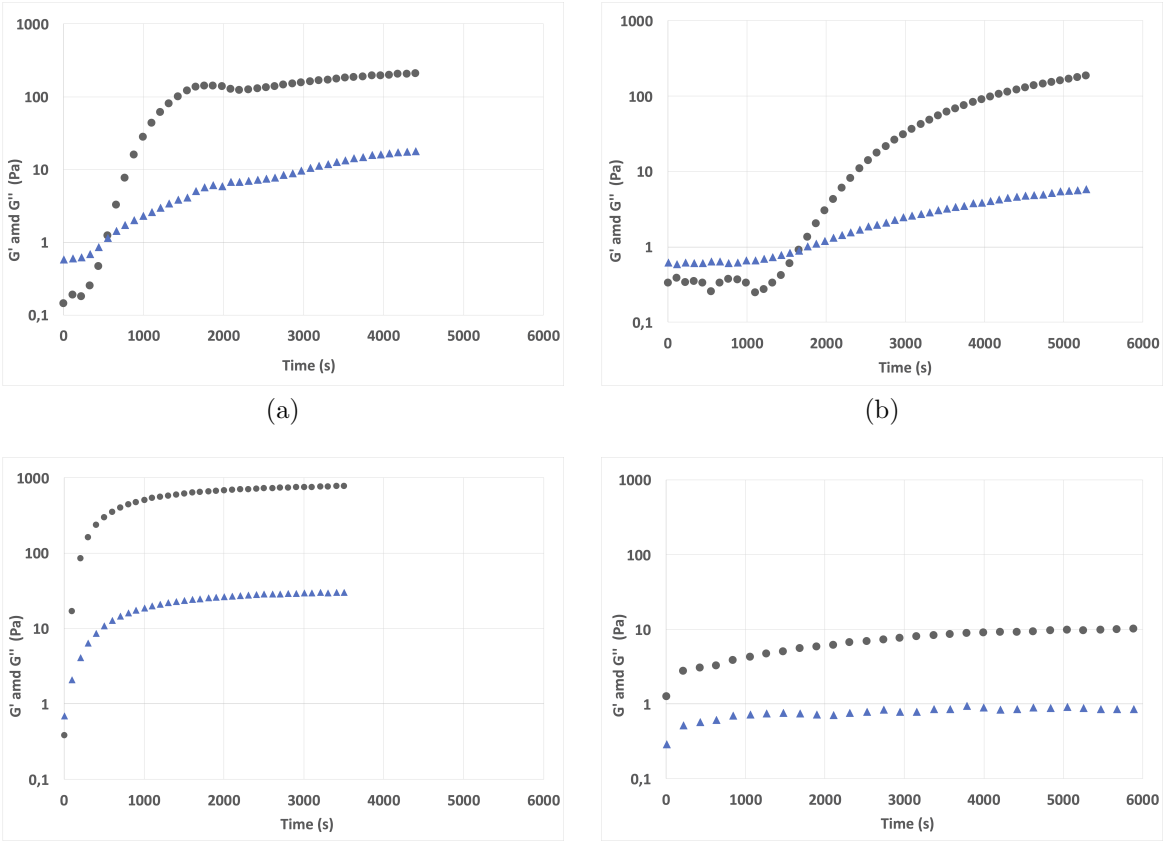

(a) (b)

(c) (d)

Figure 9: Gelation kinetics of 100 % crosslinked alginate gels with different Ca^{++} release rates: (a) Slow alginate gelation; (b) Incomplete alginate gelation; (c) fast alginate gelation; and, (d) Col-[redacted]. Grey dots and light blue triangles symbolise the storage modulus and the loss modulus respectively.

The incomplete gelation seen in figure 9b was too long resulting in sedimentation of [redacted] particles and phase separation of water and the alginate gel. Moreover, the gelation kinetics show that alginate gelation occurs more rapidly than collagen only in the case of using the fast gelation rate, as seen in figure 9c, possibly allowing for collagen to use alginate as a template when forming a network. Therefore, in the subsequent trials this method of Ca^{++} release was utilised.

4.4 Alg-Col gels with rapid Ca^{++} release - Gelation kinetics

The gelation curves of col-alg gels with 50 % alginate crosslinking degree compared with pure alg gels are presented in figure 10 below.

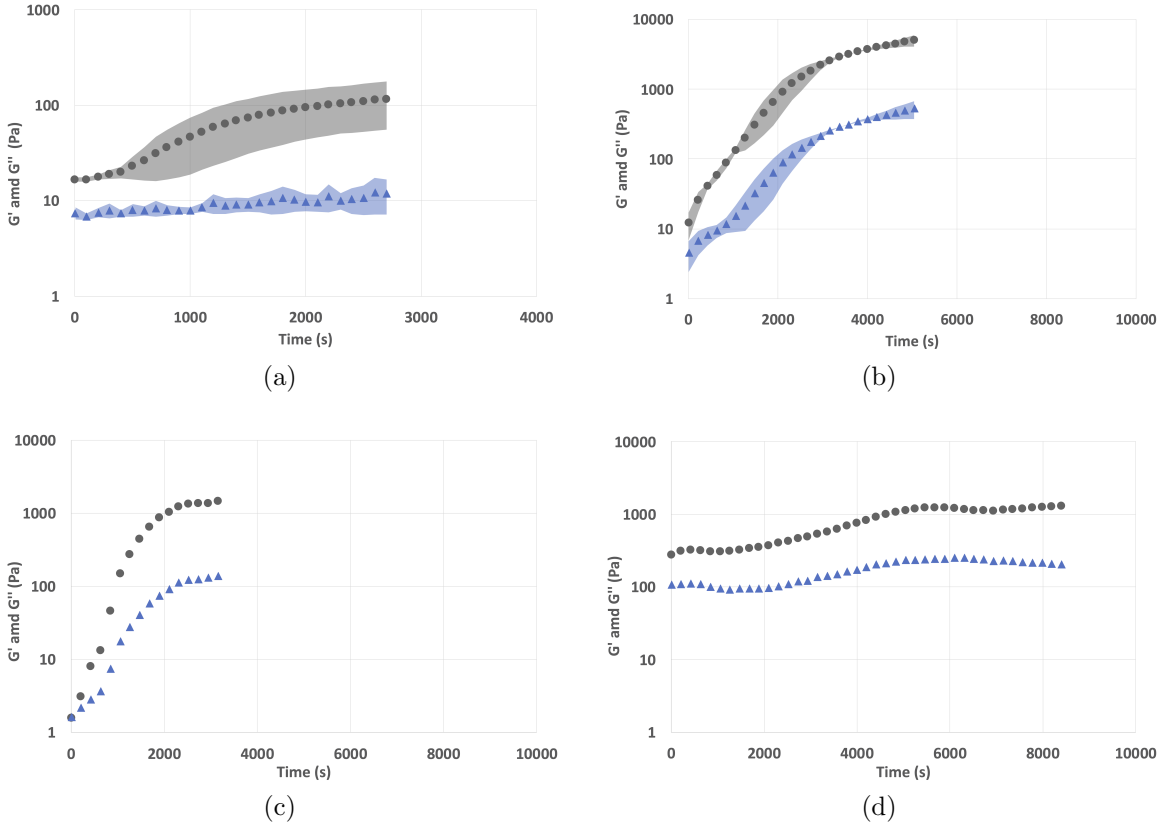

Figure 10: Gelation kinetics of Alg-Col-[redacted] gels with rapid Ca^{++} release: (a) Alg-Col-[redacted]; (b) Alg-Col-[redacted]; (c) Alg-Col-[redacted]; and, (d) Alg-Col-[redacted]. Grey dots and light blue triangles symbolise the storage modulus and the loss modulus respectively. The coloured area around the datapoints represents the standard deviation of the modulus.

The gelation curves of col-alg gels with 100 % alginate crosslinking degree compared with pure alg gels are visualized in figure 11

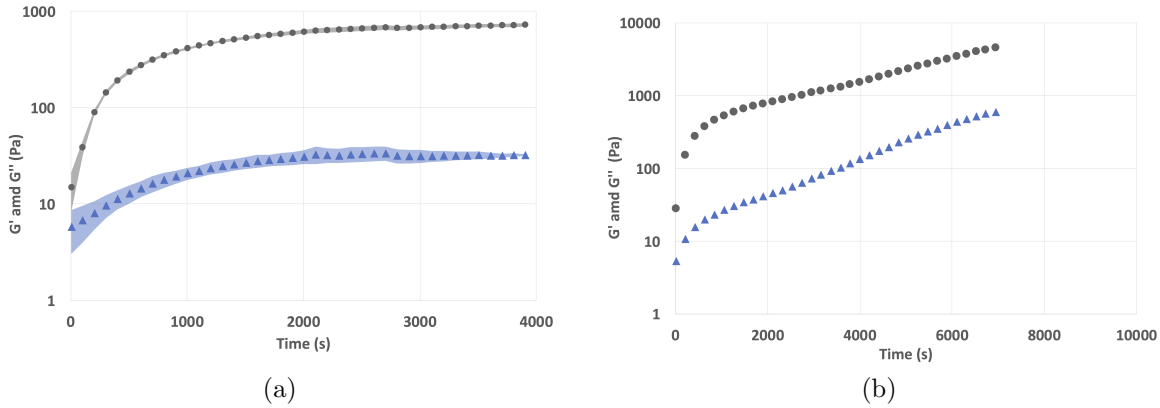

Figure 11: Gelation kinetics of Alg-Col-[redacted] gels with [redacted] Ca^{++}: (a) Alg-Col-[redacted] and (b) Alg-Col-[redacted]. The coloured area around the datapoints represents the standard deviation of the modulus.

As apparent in the graphs of figure 10 and 11, the gelation process of the col-alg gels is considerably longer compared to the pure alginate gels. Moreover, specifically comparing 11a with 10a, it is apparent that the 100 % crosslinked alginate gels exhibit a roughly 10-fold higher shear strength compared to the 50 % crosslinked alginate gel, which is expected based on previous studies as discussed in section 2.2. A general trend is that the col-alg gels exhibit different viscoelastic properties compared to the pure alginate gels, a difference whose consequences became apparent during cell loading as discussed in section 4.9. All combined col-alg gels exhibit a characteristic kink in their gelation curves, except the col-alg gel with 100 % alginate crosslinking in figure 11b, possibly indicating the point at which significant fibrillogenesis is initiated in the alginate network. Based on the impact of varying the collagen concentration and [redacted] on the gelation kinetics there appears to be a synergistic effect on the shear modulus. In particular, this is evident when comparing figure 10a with 10c and 7c, highlighting how the final shear modulus recorded is close to 100-fold higher for the Alg-Col gel compared to the pure alginate gel, which in turn has a 10-fold higher shear modulus than the pure collagen gel.

This is expected as collagen predominantly contributes to torsional stability, i.e. shear strength, in native articular cartilage, as previously discussed in section 2.1. However, it appears that this effect is more pronounced at 50 % alginate crosslinking, possibly indicating that collagen is confined between the alginate at higher crosslinking degrees due to the faster gelation rate. The formation of such islands rather than an IPN would explain a less synergistic interaction at higher crosslinking degrees.

4.5 Alg-Col gels with rapid Ca^{++} release - Frequency sweeps

All gels containing alginate are defined as strong gels where the G' and G" moduli are relatively independent of frequency for up to 60 hz. The addition of collagen did not change this behaviour. For complete graphs of the frequency sweeps see appendix B. A weak power function explaining the relation between the storage modulus and the frequency and a much lower loss modulus, which is observed in all cases, is also what has previously been reported for alginate and alginate-collagen gels as mentioned in section 4.8.

4.6 Swelling trials

The reference alginate gels appeared to be slightly firmer than those with collagen during initial cell trials. Swelling trials were therefore subsequently performed to assess the hydrogels stability as initial experiments with cells suggested lower structural integrity among the gels containing collagen. The reported mass changes are presented in figure 12 below.

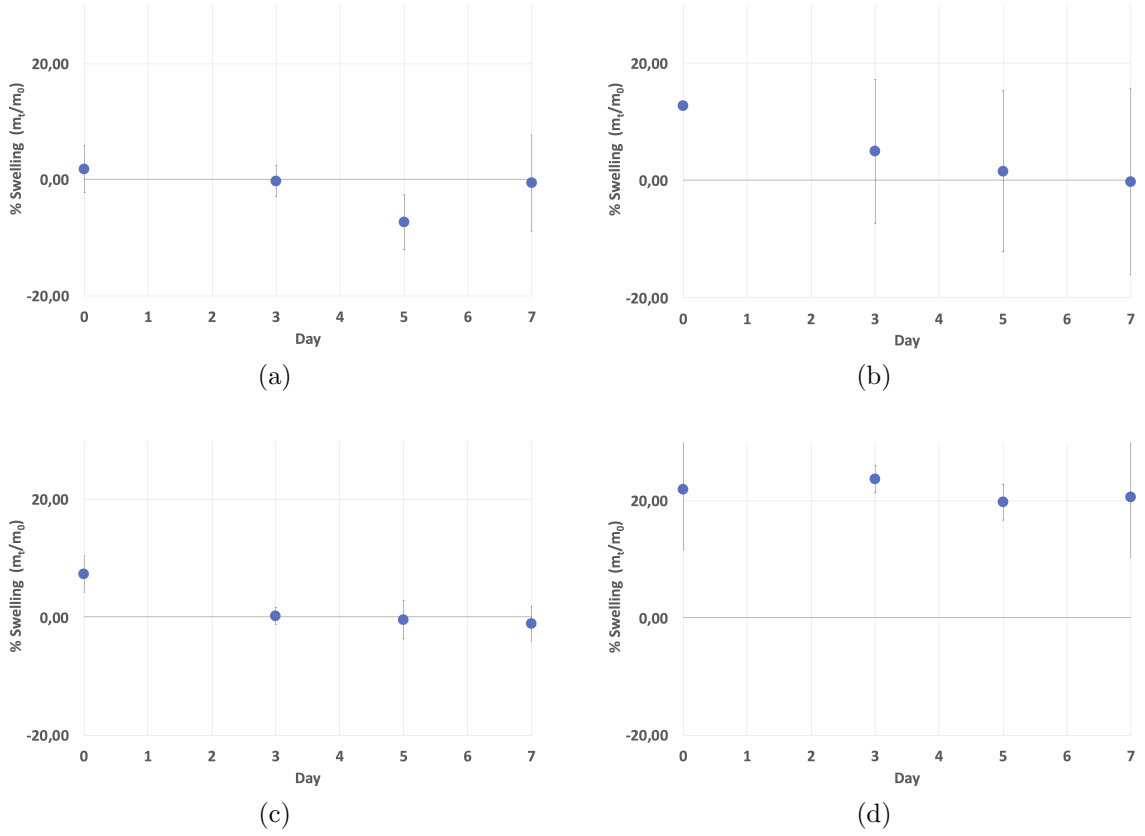

Figure 12: Swelling trials of Alg-Col-[redacted] gels with [redacted] Ca^{++}. Measures of mass change: (a) Alg-Col-[redacted]; (b) Alg-Col-[redacted]; (c) Alg-Col-[redacted] and (d) Alg-Col-[redacted].

All gel formulations except Alg-100 did not change significantly in mass during the week (ANOVA, Tukey's *post-hoc* test), suggesting that the addition of new ions in the solutions when replacing the media was not enough to cause dissolution or significant destabilisation of the gel structures which, given enough time, should occur due to the ion exchange as described in section 2.3. Alg-100 however dropped significantly in mass day one through day five. Even on the first day, the mass of the gels did not change significantly, which should be the case if swelling occurs. This is also expected as the constitution of the gels is very similar to that of the surrounding nutrient solution, i.e the difference in chemical potential is low, and therefore inflow of water should be minimal and not cause significant swelling. The data observed is in line with what has previously been reported for alginate-collagen gels. The volumetric changes saw greater variance and are less reliable due to the lack of adequate equipment for measuring with accuracy. For application as a chondrocyte scaffold, the study should be extended to include at least 4 weeks of data as this is the time frame within which substantial ECM production is expected to occur and thus requires gel to keep its structural integrity as discussed in section 2.3.

4.7 Large deformations of gels with rapid Ca^{++} release

It had not yet been verified whether the synergistic torsional strength observed for the alginate-collagen gels would translate to improved axial compression. Results from fracture stress tests presented below in figure 13.

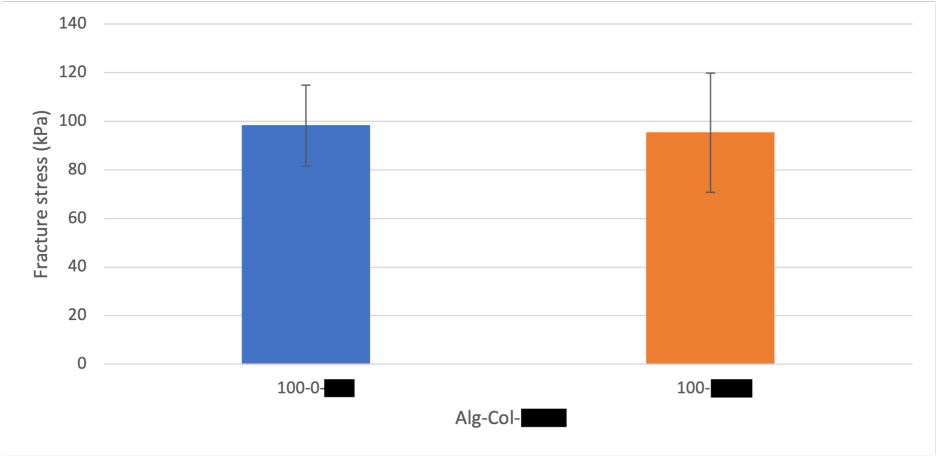

Figure 13: Comparison of breaking strengths of 5x5 mm alg and col-alg gels with fast gelation.

No significant difference in mean fracture stress was detected (two-sided t-test). However, when comparing the elastic Young's modulus a significant improvement was observed (two-sided t-test), as seen in figure 14.

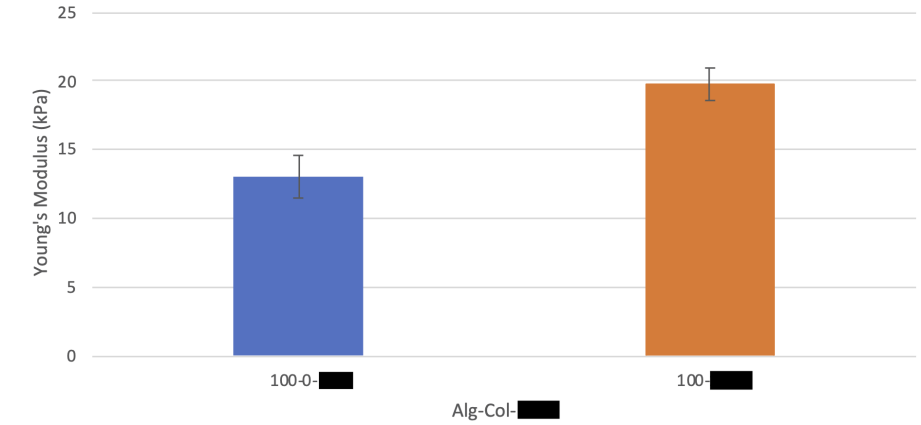

Figure 14: Comparison of Young's modulus of 5x5 mm alg and col-alg gels with fast gelation.

In order to investigate the impact of changing the temperature to one geared towards optimal [redacted] [redacted] rather than collagen fibrillogenesis, a gelation was also carried out at room temperature. The resulting breaking strengths compared to alginate reference gels are presented in figure 15.

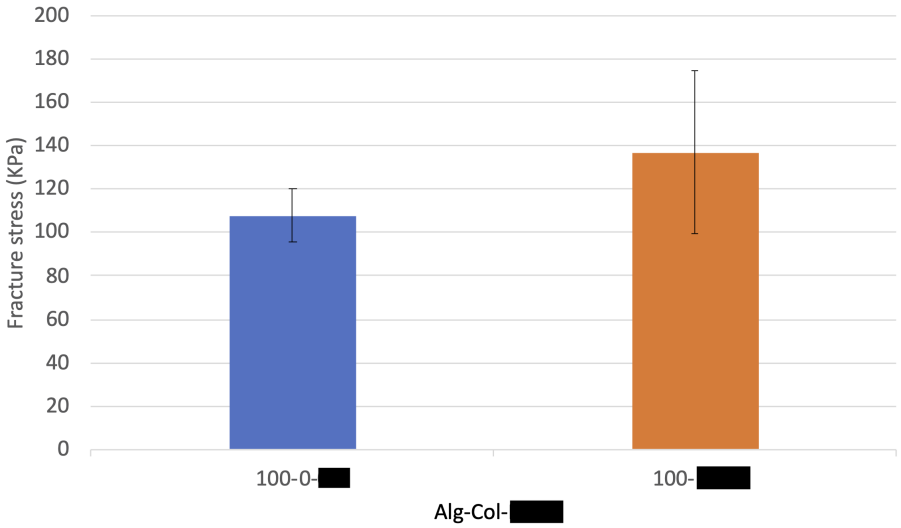

Figure 15: Comparison of breaking strengths of 5x5 mm alg and col-alg gels with fast gelation which has been allowed to solidify at room temperature.

No significant difference in the average breaking strength was observed (two-sided t-test). When comparing the elastic Young's modulus, presented in figure 16 below, once again a significant improvement is observed.

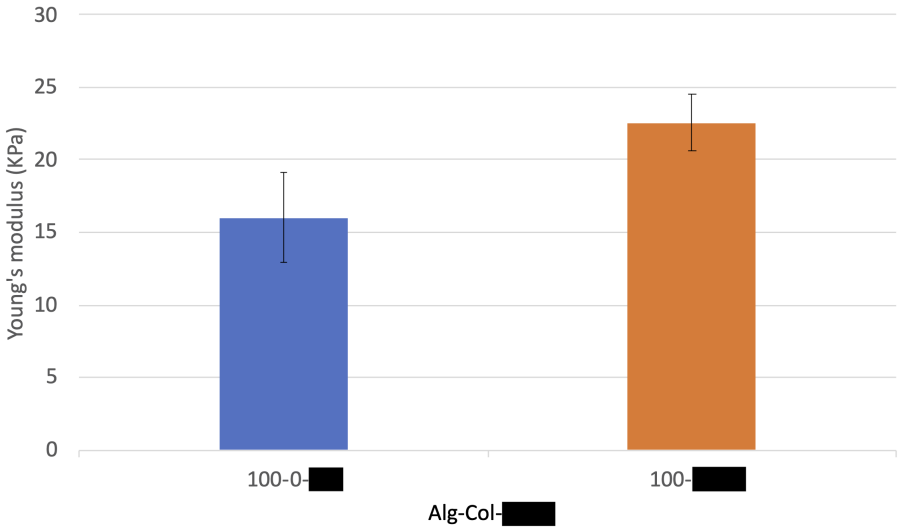

Figure 16: Comparison of Young's modulus of 5x5 mm alg and col-alg gels which has been allowed to solidify at room temperature.

4.8 Fluorescent imaging of gels with rapid Ca^{++} release

The lack of an IPN, as defined in section , was then confirmed by fluorescent imaging as seen in figure 17 below.

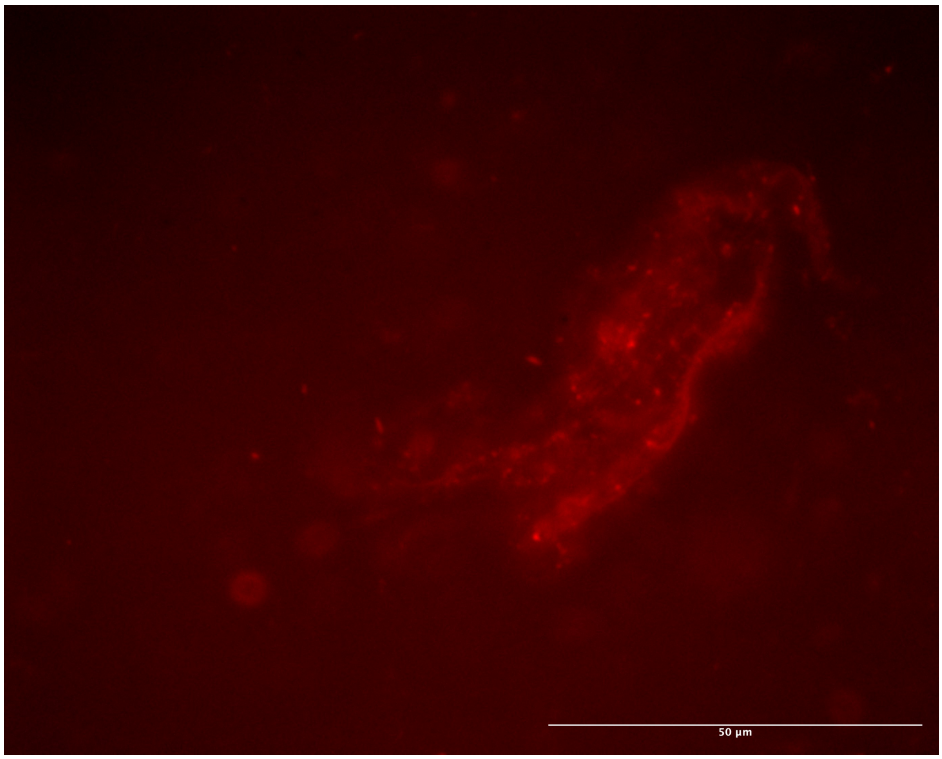

Figure 17: Fluorescent image of a [redacted] *Alg-Col-*[redacted] *gel section stained with 1 % Eosin B and observed through a 100x magnification oil immersion lense*

The figure shows an aggregated collagen cluster within the alginate network, a pattern that was seen sporadically throughout the entire gel slice.

4.9 Cell loading of gels - Cell density & viability

In early trials with cells a dispersion of cell pellets were mixed with the alginate and collagen solutions immediately upon introduction of the gelling components, in an attempt to achieve a homogenous distribution. This method saw low viability among the dispersed individual cells as visualised by live/dead imaging in figure 18 below. Dots with a bright shine represent cells whereas cloudy areas is caused by the spread of light passing through the gel. Green and red represent living and dead cells respectively.

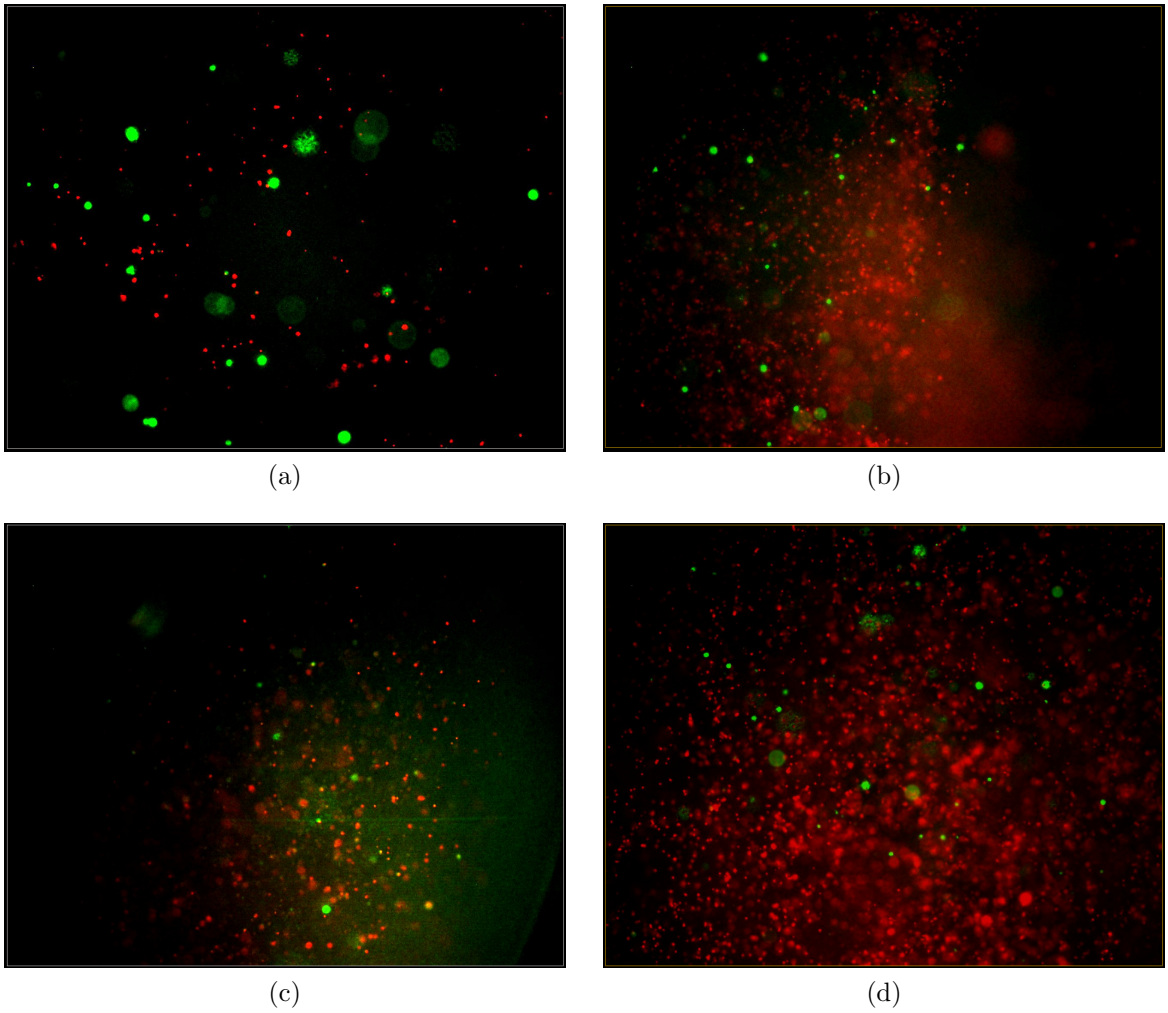

Figure 18: Live/dead imaging of dispersed cells in hydrogels: (a) Alg-Col-[redacted] day 3; (b) Alg-Col-[redacted] day 3; (c) ; Alg-Col-[redacted] day 7, (d) Alg-Col-[redacted] day 7

As observed when comparing gels with and without collagen the viability is much lower in the latter, with a majority of the cells escaping the matrix to the bottom of the well as represented by the cloudy red areas. The cells escaping can likely be explained by the slower gelation rate of the collagen containing gels as discussed in section 4.4. The few larger clusters which had stayed intact during the vigorous mixing demonstrated a higher survival rate which is particularly apparent when looking at figure 18a.

The second round of trials once again saw issues with a majority of the cells escaping from the scaffold, possibly attributed to the gel rupturing in connection with the cell injection due to the fast gelation rate. Due to this and the lack of an IPN, [redacted] was chosen in favour of [redacted] for subsequent trials owing to its much slower gelation rate as evident in figure 9. This would allow for controlled integration of a larger cell pellet post gelation. Furthermore, it was suggested that the slower gelation rate of the alginate might provide necessary time needed for the collagen network to develop before the viscosity could prevent further fibrillogenesis from occurring. The following cell trials demonstrated much improved viability as expected. Live/dead

imaging 2 days post cell integration is presented in figure 19 below. It should be noted that a new set of cells are stained for each round which makes comparison of the same gel type over time difficult.

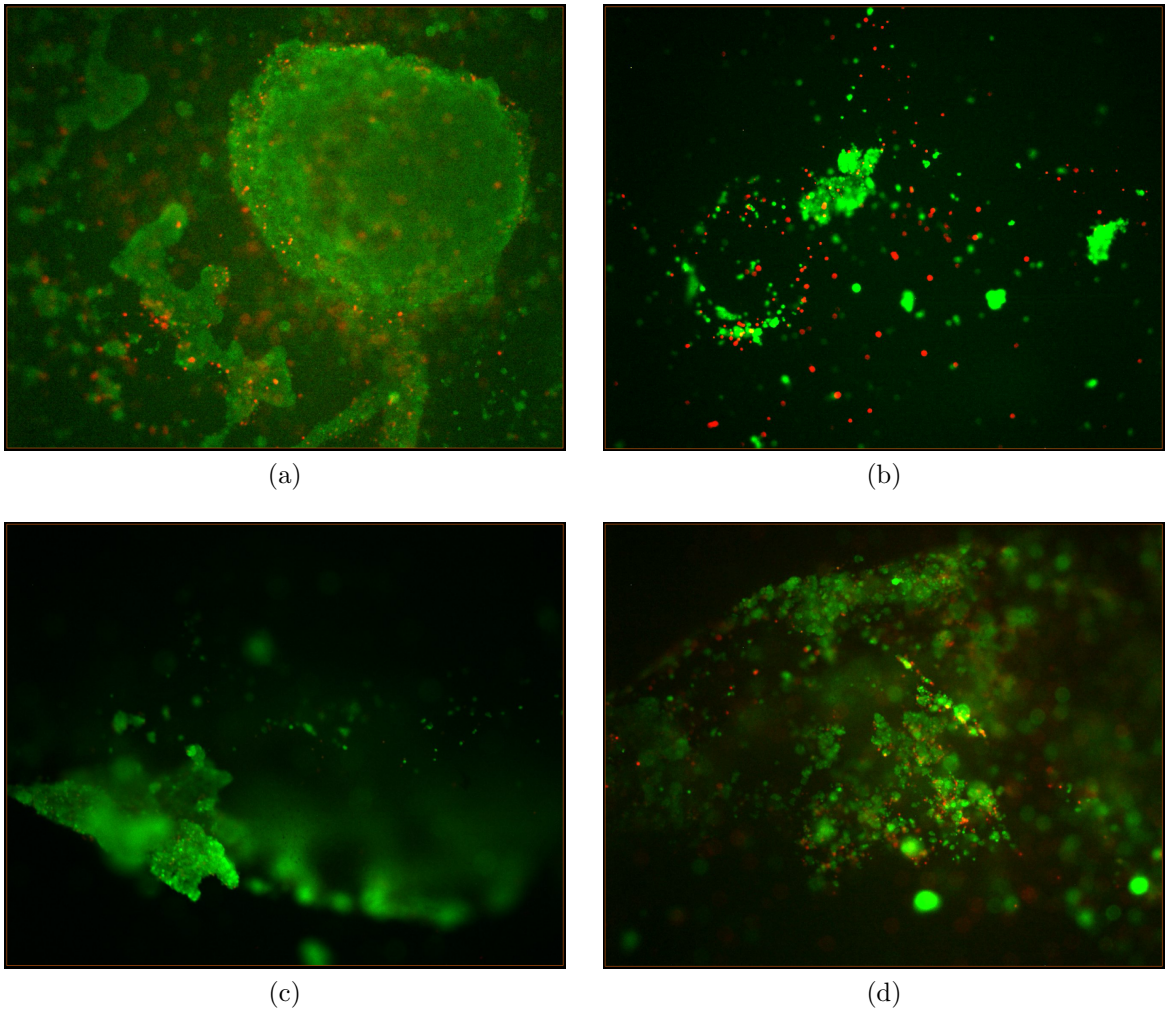

(a) (b) (c) (d)

Figure 19: Live/dead imaging of cell pellets integrated into hydrogels, 5XPH1 objective lens, day 2: (a) Alg-Col- gels with cell integration by ; (b) Alg-Col- gels with cell integration by ; (c) ; Alg-Col- with cell integration by , (d) Alg-Col- gels with cell integration by

The method in the pure alginate hydrogels resulted in the most intact cell pellets, as observed when comparing 19a to the remaining figures. The method was less effective at keeping the cells together as apparent when comparing figure 19a with 19d. Finally both gels containing collagen demonstrated a greater spread and fractionation of the cell clusters as particularly evident when comparing 19a with 19b. The greater spread of the cells in the collagen containing gels could in part be attributed to the greater viscous portion of the gels as discussed in section 4.4. However, in all cases, the cell loss was much lower compared to the previous trials, demonstrating the advantage of using as Ca^{++} source compared to . Figure 20 below demonstrates viability and cell distribution 7 days

post integration.

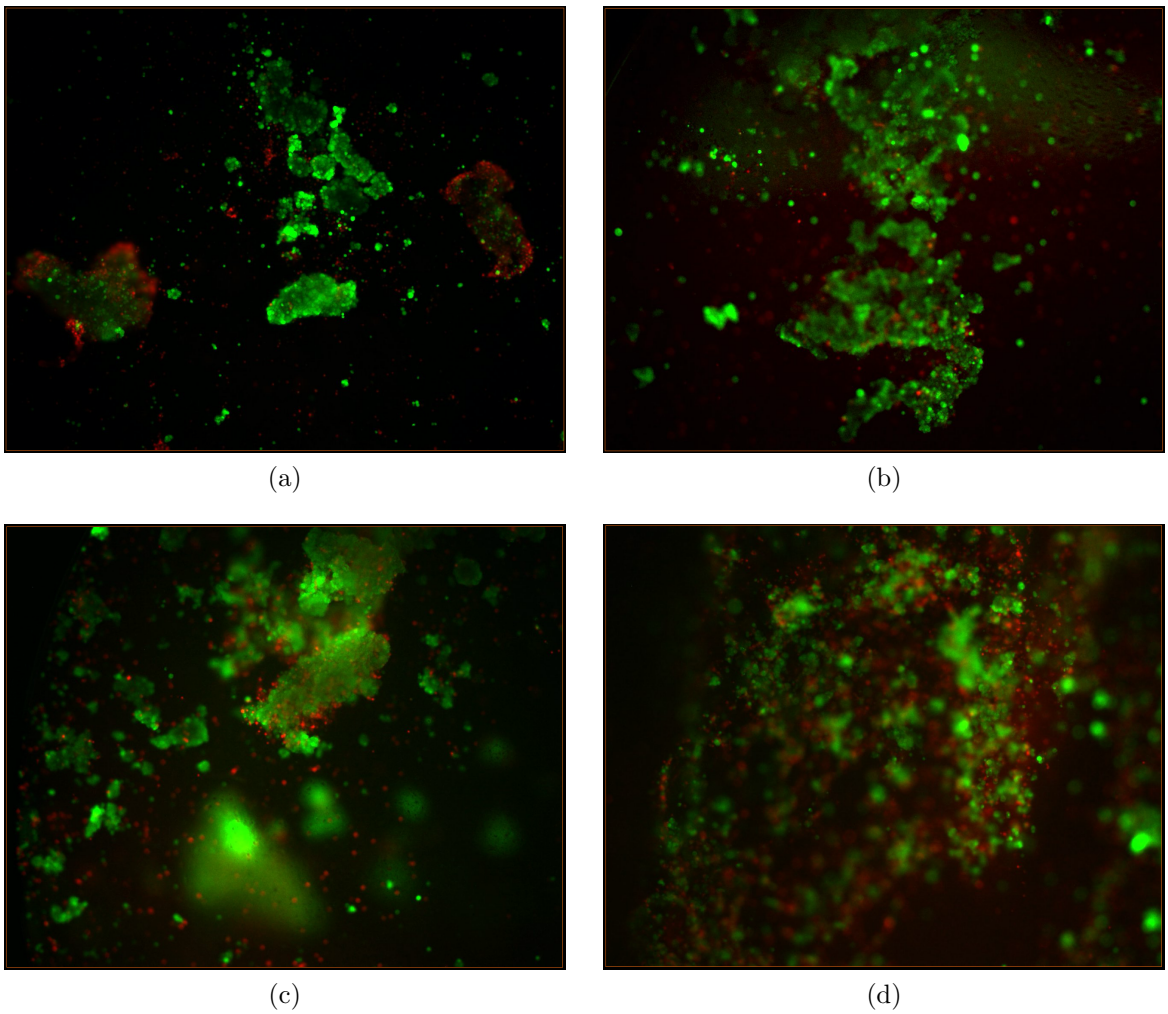

(a) (b)

(c) (d)

Figure 20: Live/dead imaging of cell pellets integrated into hydrogels, 5XPH1 objective lens, day 7: (a) Alg-Col- gels with cell integration by ; (b) Alg-Col- gels with cell integration by ; (c) ; Alg-Col- gels with cell integration by , (d) Alg-Col- gels with cell integration by

The viability was still fairly high for a gel types and cell loading methods 7 days post integration as shown in figure 20. The superiority of the method is still evident in particular when comparing the two collagen gels in figure 20b and 20d respectively. Figure 21 finally visualises viability results 14 days post integration.

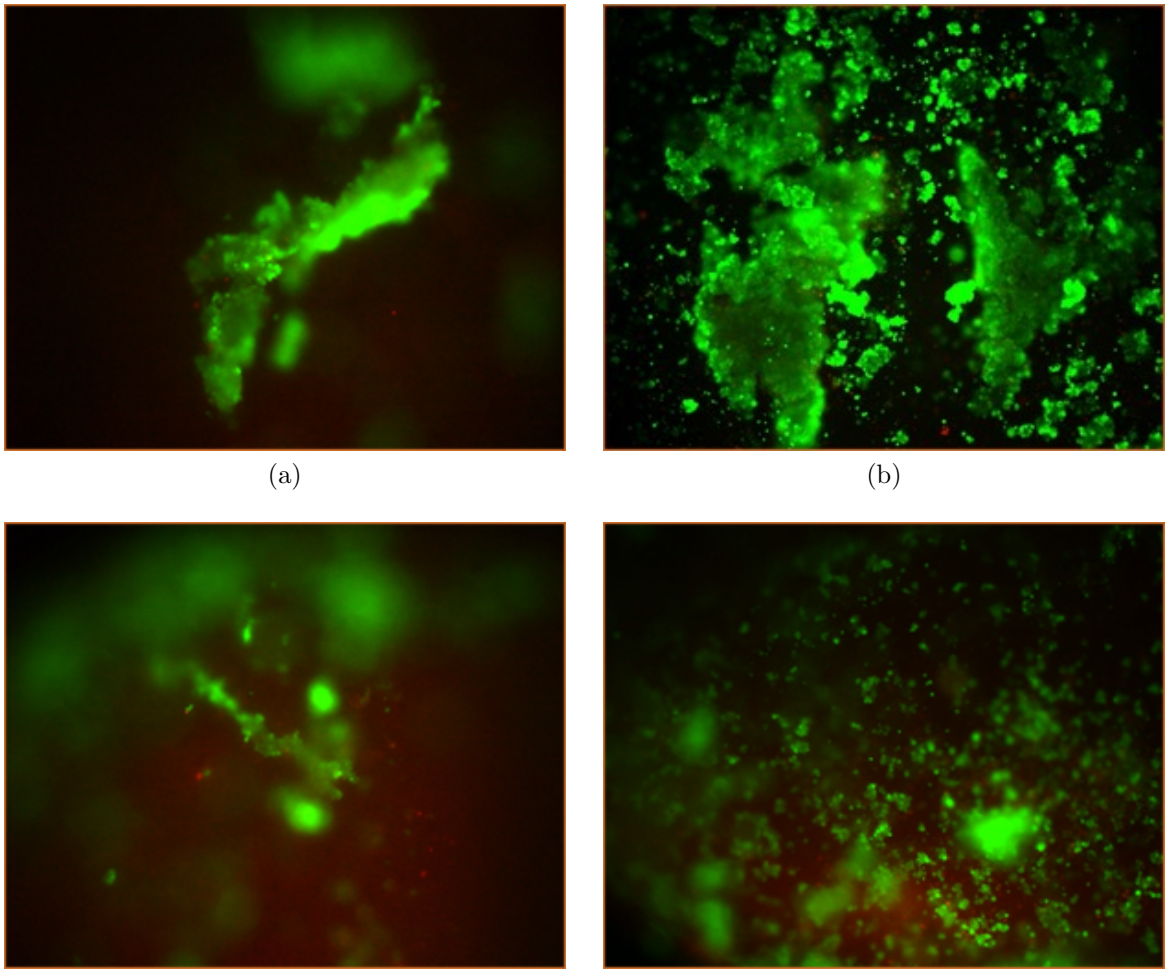

(a) (b)

(c) (d)

Figure 21: Live/dead imaging of cell pellets integrated into hydrogels, 5XPH1 objective lens, day 14: (a) Alg-Col- gels with cell integration by ; (b) Alg-Col- gels with cell integration by ; (c) ; Alg-Col- gels with cell integration by , (d) Alg-Col- gels with cell integration by

Once again the advantage of the method is apparent with viability being greater in both cases as seen when comparing figure 21a and 21b with

4.10 Large deformations of gels with slow Ca^{++} release

Figure 22, 24, 23 and 25 below presents interval plots of important characteristics collected from unconfined compression trials including fracture stress and strain, toughness and Young's modulus.

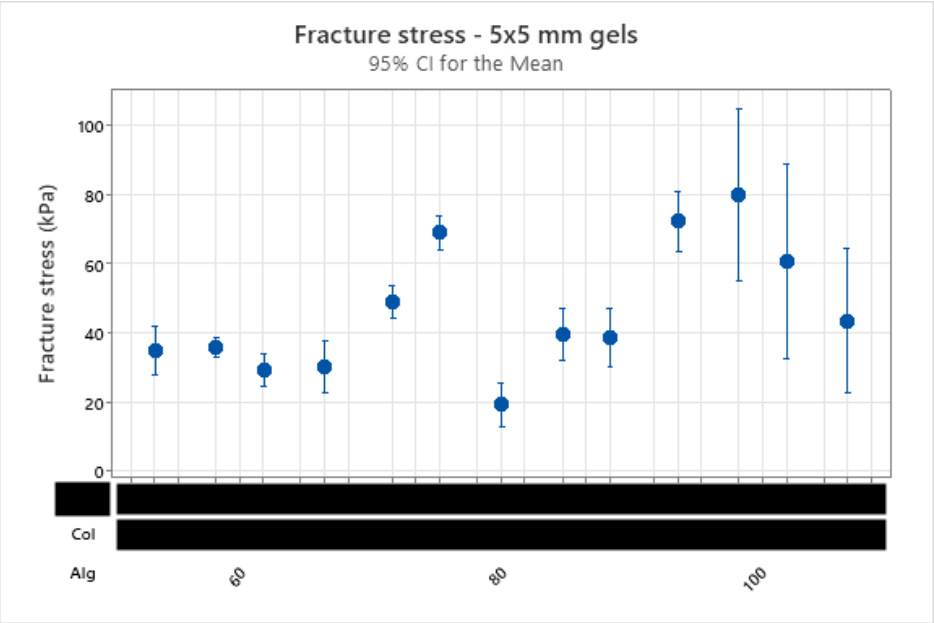

Figure 22: Unconfined compression of gels with slow Ca^{++} release: Interval plot of fracture stress

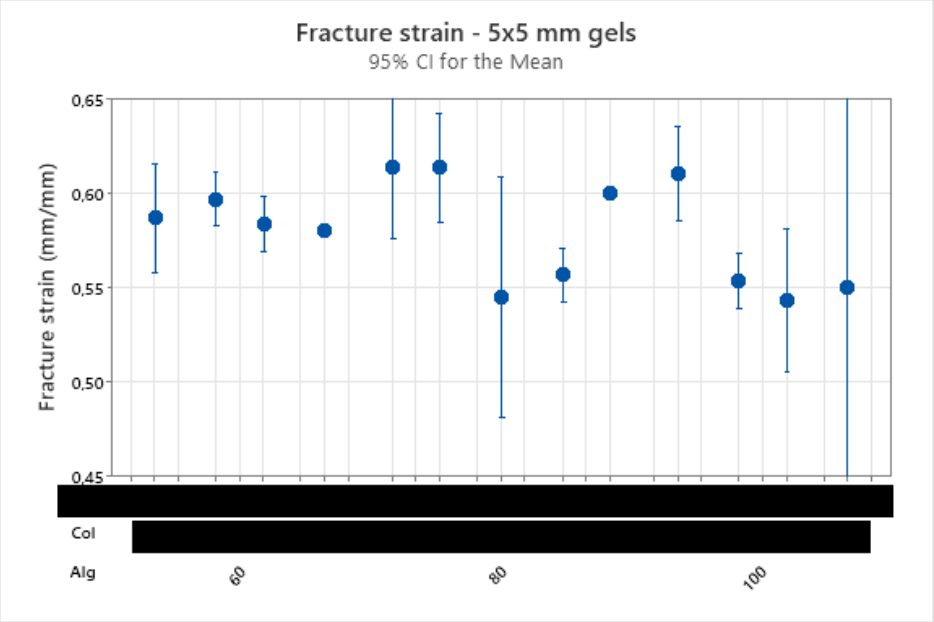

Figure 23: Unconfined compression of gels with slow Ca^{++} release: Interval plot of fracture strain

As evident from the graph the gel formulation has little impact on the fracture strain, including the alginate cross linking degree, which is in line with previous studies as discussed in section 2.2. However, a slight and negative influence of the alginate crosslinking degree, the collagen concentration and their interaction on the fracture strain was detected by regression analysis (see appendix C.2 for the complete regression models). A slight positive influence was observed for the quadratic [redacted] term.

However, being in the order of 1 % difference in deformation between the low and high levels of the respective components, the impact is negligible for practical applications.

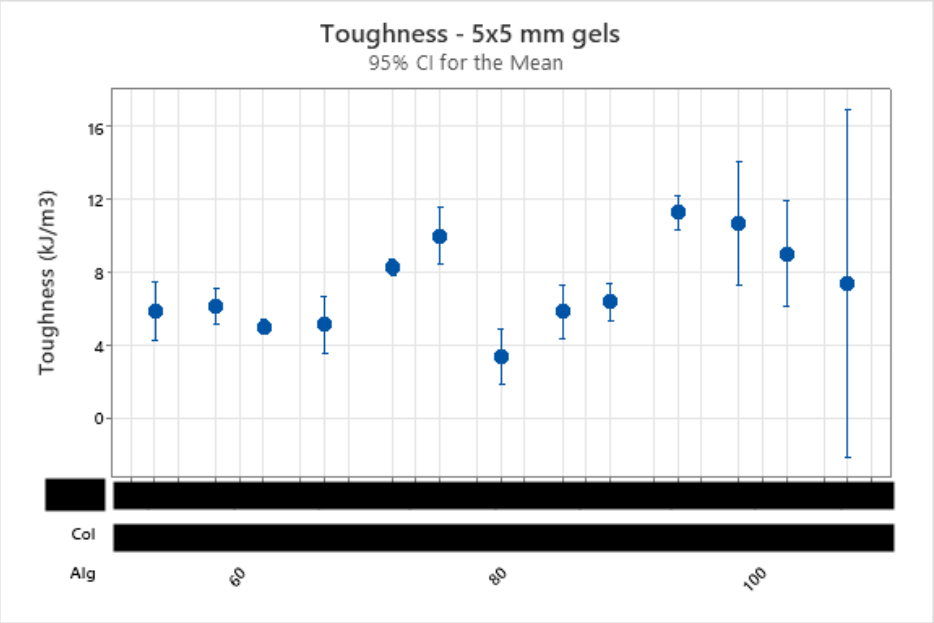

Figure 24: Unconfined compression of gels with slow Ca^{++} release: Interval plot of toughness

As evident from figure 22 and 24, the fracture stress and the toughness of the gels are highly correlated as indicated by the similarly shaped curves that the datapoints of the different gel formulations constitute.

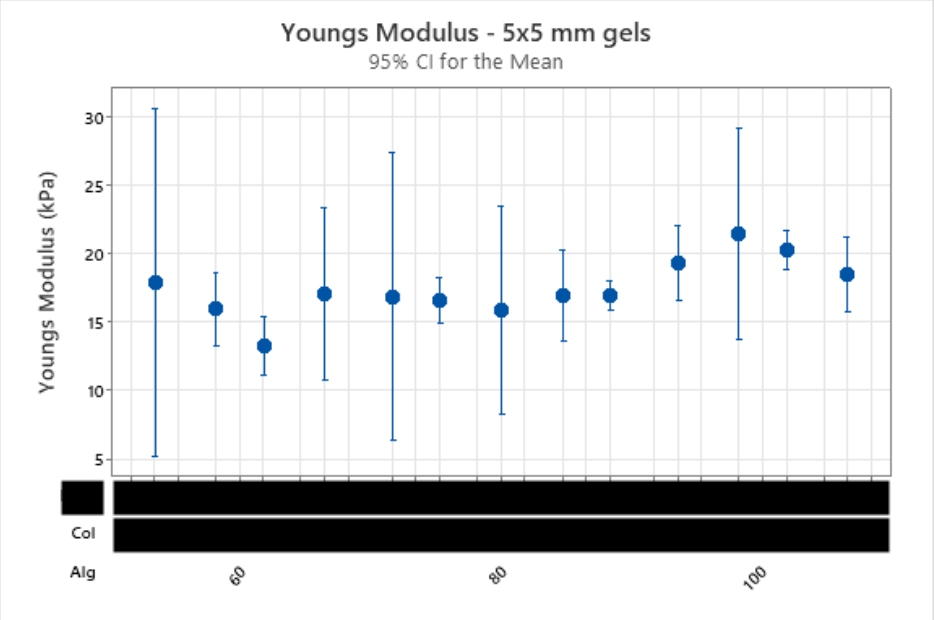

Figure 25: Unconfined compression of gels with slow Ca^{++} release: Interval plot of Youngs modulus

Young's modulus shows a different trend and appears to be mainly dictated by the alginate crosslinking degree as seen in figure 25. The observed values are similar to what has previously been reported for calcium-crosslinked alginate gels during unconfined compression as discussed in 2.2. In the following figure, the associated maximum elastic strains of the gels in the LVR are presented.

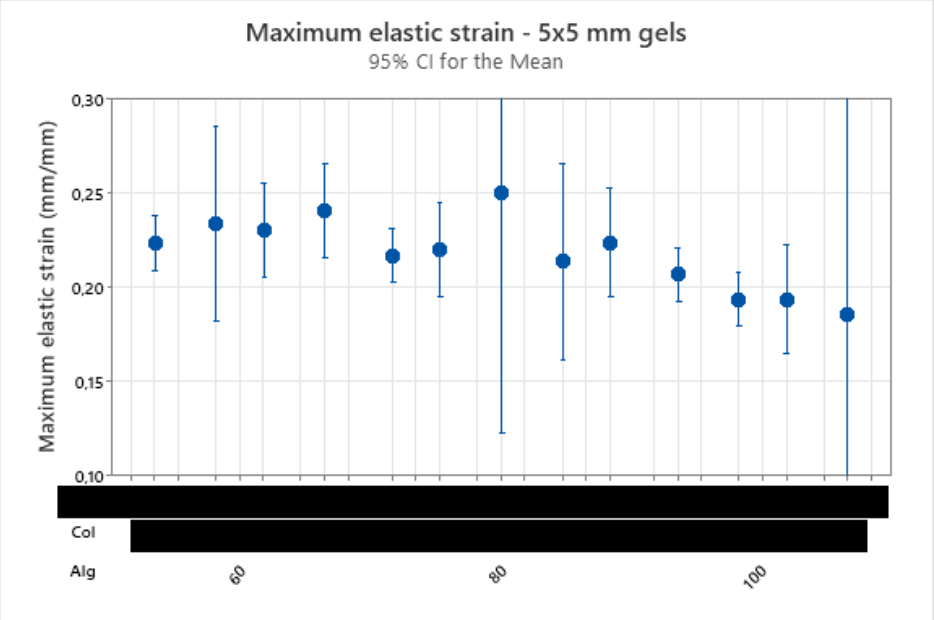

Figure 26: Unconfined compression of gels with slow Ca^{++} release: Interval plot of maximum elastic strain

Noticeably, the physiological deformations of articular cartilage, as presented section 2.1, falls well within the LVR of all gel formulations. The alginate crosslinking degree and collagen concentration as well as their interaction demonstrated a slight but significant negative influence on the maximum elastic strain, in contrast to the Young's modulus, as evaluated by regression analysis (see appendix C.5 for complete regression models). The quadratic [redacted] term also demonstrated a slight negative impact. However, once again being in the order of 1-2 % difference in deformation between the low and high levels of the respective components, the impact is considered to be negligible in practice.

Regression models were made for each case to more closely inspect the influence of the gel components, i.e. alginate (alg), collagen (col) and [redacted]. For each response, both a complete quadratic and a reduced model based on stepwise elimination of terms with $\alpha \leq 0.05$ were made.

Both in the case of fracture stress and toughness, as expected, the alginate terms has a positive influence on the mechanical performance. See appendix C.1 and C.3 for complete data on each model. For fracture stress the negative influence of the collagen is more pronounced as seen when comparing figure S4 and S6. In both cases the fit and predictability of the model is quite good as indicated by the R^2 values in the model summary. Associated surface plots are presented in figure 27 below, highlighting the

influence of collagen concentration and alginate crosslinking degree on fracture stress and toughness as identified by the regression models.

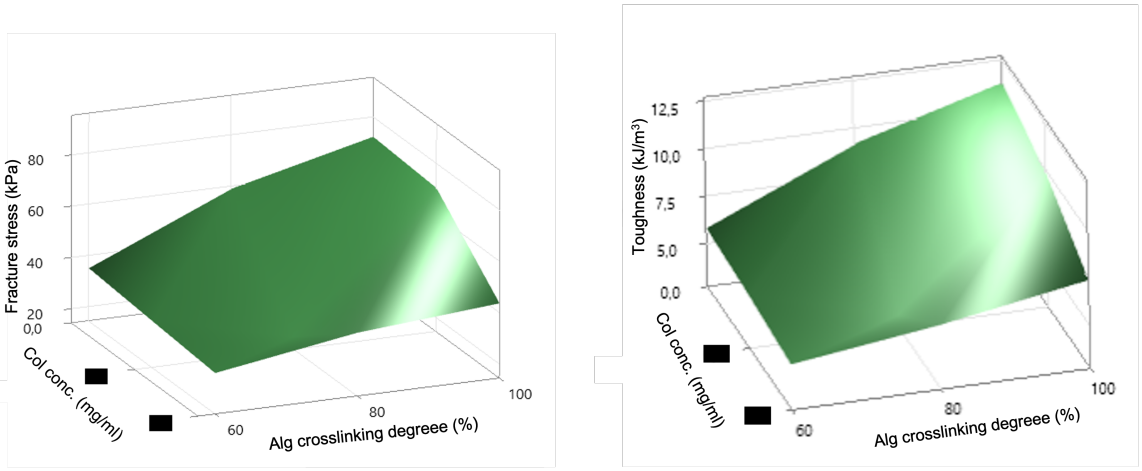

(a) (b)

Figure 27: Surface plots of collagen concentration and alginate crosslinking degree influence on: (a) fracture stress and (b) toughness

Once again the positive and negative influence with increasing alginate crosslinking degree and collagen concentration respectively in both cases is evident as indicated by the slope of the surface plots.

Finally, a regression model was also made for the Young's modulus. As indicated by the confidence interval plot in figure S7, only alginate had a significant impact on Young's modulus. The fit of the model is poor however, with an R^2-adjusted of 28,68 %. This indicates that batch-to-batch variability in the gel manufacturing procedure and other unknown factors explains the vast majority of the variance seen in Young's modulus. Complete data of the regression model can be found in appendix C.4.

4.11 Stress relaxation of gels with slow Ca^{++} release

The elastic deformation of the gels was further investigated by conducting stress relaxation tests in the rheometer. Following 4 minutes of stress relaxation the stress responses had become fairly stabilised in all cases. Stresses at small deformations, more specifically those of order 100 Pa, are close to the sensitivity limit of the rheometer and are therefore not as reliable. In figure 28 below the stress responses of 5x5 mm alginate gels at different degrees of deformation pre and post stress relaxation are presented.

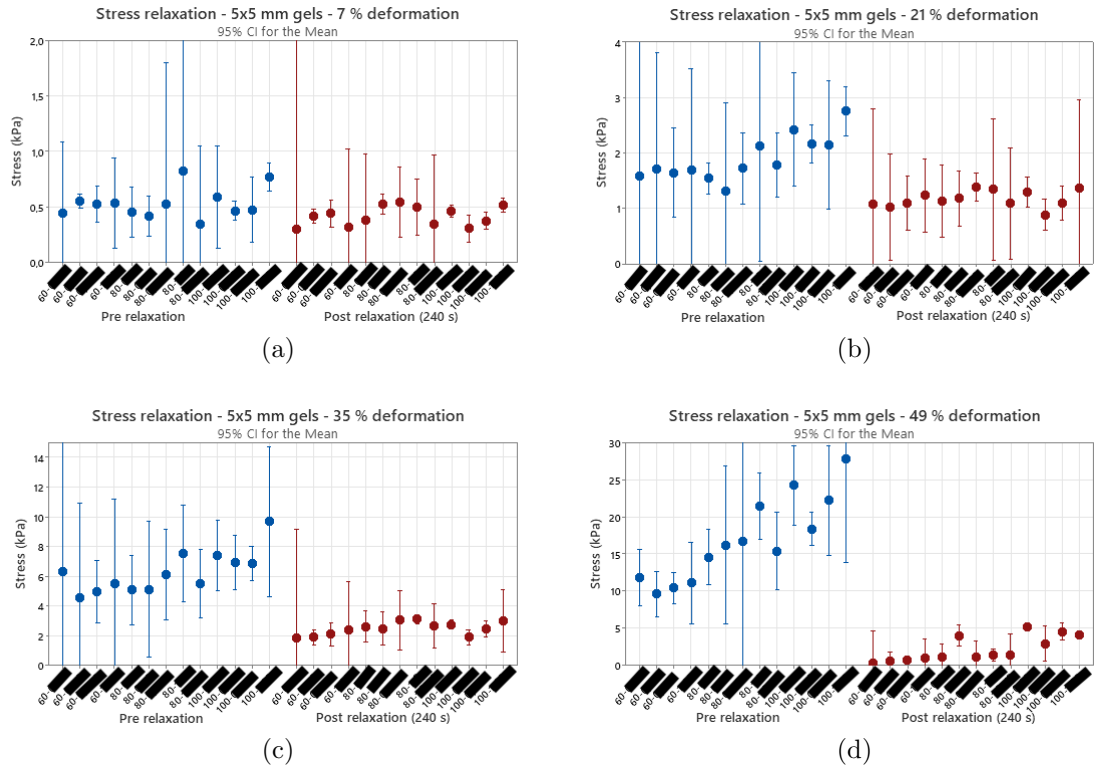

Figure 28: Stress relaxation of 5x5 mm gels with slow Ca^{++} release: (a) 7 % deformation; (b) 21 % deformation; (c) ; 35 % deformation and, (d) 49 % deformation.

At 49 % deformation, regression analysis suggests that mainly increasing the alginate crosslinking degree has a significant positive influence on the initial stress observed following compression as evident when looking at the trend in figure 28d. Additionally, regression analysis indicates that the alginate crosslinking degree has a positive influence on stress observed post relaxation, whereas the influence of the [redacted] and collagen concentration varies with the formulations. Lastly, the alginate crosslinking degree was also found to have a positive impact on the reduction in stress observed post relaxation compared to the initial stress, i.e. the stress relaxation time. Up to roughly a 15-fold decrease in the compressive strength is observed post relaxation, similar to what has been reported for articular cartilage during unconfined compression as discussed in section 2.1. The influence of [redacted] varies with the formulations whereas the collagen concentration has a significantly negative interaction effect with [redacted]. See appendix C.6, C.7 and C.8 respectively for complete regression models. At the lower deformation levels the fit of the regression models were too low to include. Alginate was the only significant factor at 21 and 35 % deformation pre relaxation. At 7 % deformation only the [redacted] interaction had a significant impact and it was slightly negative. At the lower deformation levels post relaxation only alginate had a significant impact, which was positive and observed at 35 % deformation. Alginate demonstrated a negative impact at the lower deformation levels with regards to the stress relaxation times, i.e. gels with higher alginate crosslinking degrees were more viscoelastic. This is unexpected as only the alginate MW should influence the viscoelasticity of the gel as mention in section 2.2. The stress relaxation half times were

in most cases >240s at 21 % deformation for gels with alginate crosslinking degree between 60-80 % which correlates fairly well with the stress relaxation time reported by Mooney et al. which is expected given the fairly similar MW used. Increasing the [redacted] increased the stress relaxation times, i.e. created more elastic gels, at 7 % deformation.

4.12 Visualisation of collagen network in Alg-Col gels with slow Ca^{++} release

In order to get a more complete picture of the issue and to verify that no IPN had been formed, fluorescent images where capture of all collagen containing gels of the experimental design. Figure 29 shows fluorescent images of 60 % crosslinked alginate-collagen gels stained with 1 % Eosin to visualise the collagen fibres.

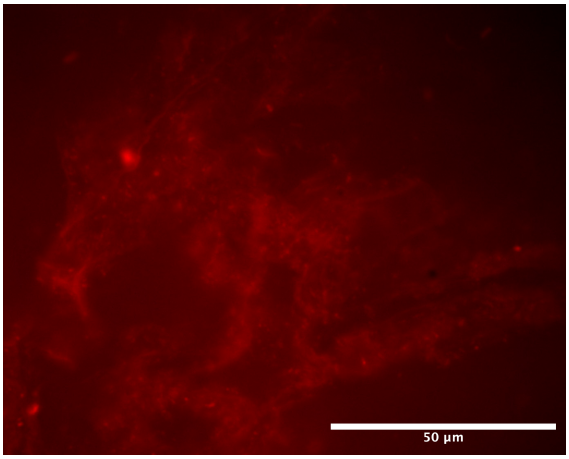

(a)

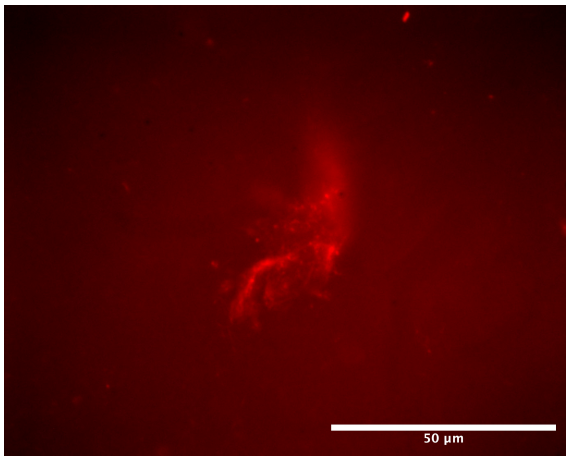

(b)

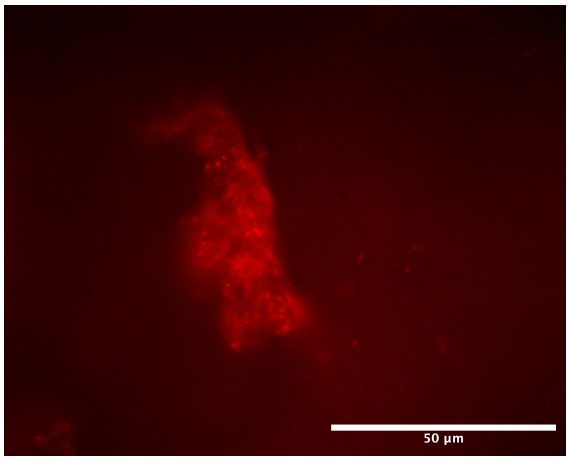

(c)

Figure 29: 5x5 mm collagen-alginate gel slices stained with 1 % Eosin B and imaged with a 100x magnification oil lense: (a) Alg-Col-[redacted]; (b) Alg-Col-[redacted]; (c) Alg-Col-[redacted]

As shown when comparing figure 29 to the pure collagen gels in figure 8, the collagen fibres have formed aggregates within the alginate gel rather than nestling in

between the alginate polymers and creating an IPN, similar to what was observed for the gels with [redacted] Ca^{++} as seen in figure 17. This was anticipated as the collagen did not have a significant positive influence on the mechanical properties of the gels as assessed by unconfined compression and stress relaxation. It should be noted that the images only represent a portion of the gel slices imaged as indicated by the length scale, since other objectives were unable to capture the collagen clusters with sufficient resolution. In each sample the aggregates were heterogeneously scattered throughout the gels only constituting a small fraction within the alginate gel landscape. The aggregates of the different gels also appeared similarly visually as evident when comparing figures 29 (a), (b) and (c).

In figure 30 below the fluorescent images of the 80 % crosslinked samples are collected.

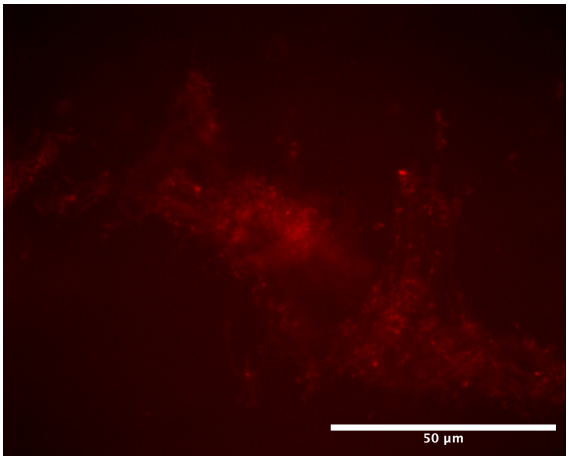

(a)

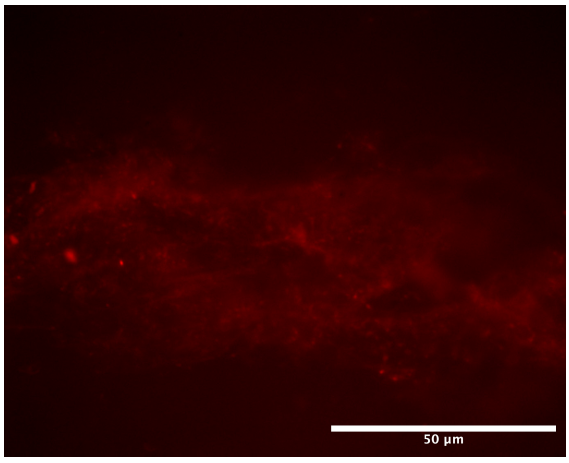

(b)

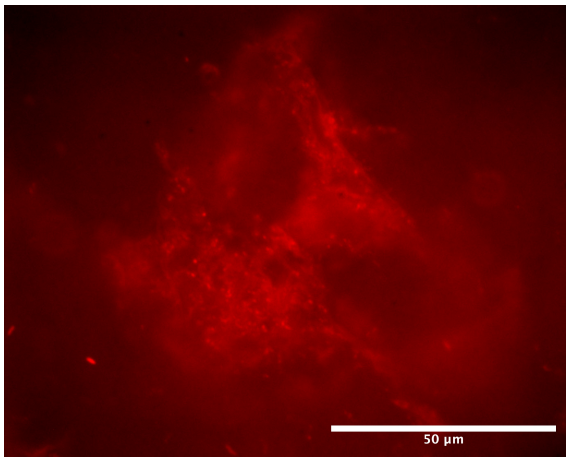

(c)

Figure 30: 5x5 mm collagen-alginate gel slices stained with 1 % Eosin B and imaged with a 100x magnification oil immersion lense: (a) Alg-Col-[redacted]; (b) Alg-Col-[redacted]; (c) Alg-Col-[redacted].

The collagen aggregates appeared visually identical to those observed in the gels with 60 %. A similar distribution in size and shape of collagen cluster scattered throughout

the gels was also observed although this could not be captured nor quantified due to the limits of the lenses available.

Lastly, in figure 30 the fluorescent images of the 100 % crosslinked samples are presented.

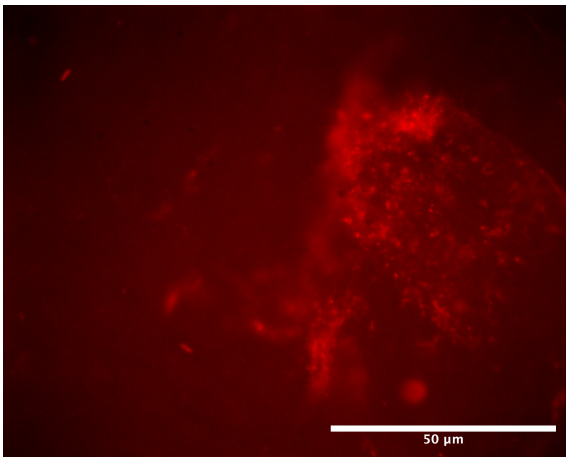

(a)

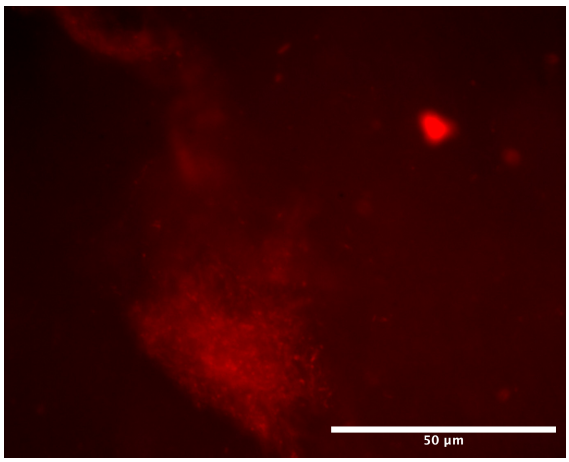

(b)

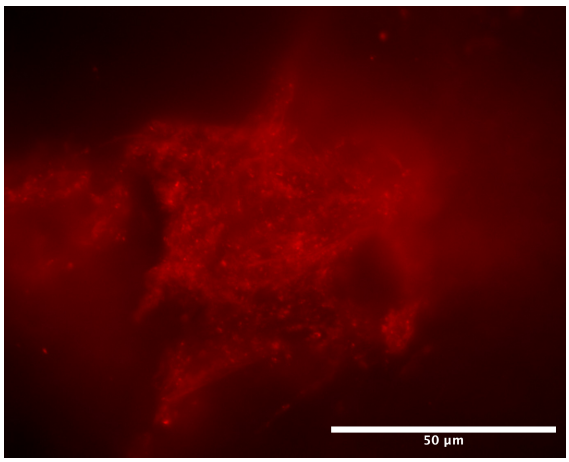

(c)

Figure 31: 5x5 mm collagen-alginate gel slices stained with 1 % Eosin B and imaged with a 100x magnification oil immersion lense: (a) Alg-Col-[redacted]; (b) Alg-Col-[redacted]; (c) Alg-Col-[redacted].

Once again the aggregates appeared visually similar to those observed at lower crosslinking degrees as seen in figure 29 and 30.

5 Discussion

As the results from the Box-Benhken design reveals, the impact of the collagen and [redacted] is slightly negative from a mechanical point of view with respective to both fracture stress and toughness. These findings are further supported by fluorescent imaging of the gels microstructure, revealing small clusters of collagen aggregates distributed within a vast space of alginate gel. This was also reflected by frequency sweeps demonstrating a relatively frequency independent behaviour of the gels. The largely frequency-independent behaviour demonstrated by the gels suggest a dominance of strong bonds over weaker physical entanglements of the network as the rearrangement of the constituent polymers should be frequency dependent. This lack of an interpenetrating network of collagen fibres and alginate polymers explains why no positive influence on the mechanical strength of the gels is seen with increasing collagen or [redacted] concentration, irrespective of the alginate crosslinking degree. In contrast, the slight but significant decrease in strength observed for the collagen containing gels is also in line with the microstructure findings as the collagen aggregates might act as a type of particulate inactive filler which typically reduce gel strength. This could also explain why the collagen does not interfere with Young's modulus as the presence of a filler would not necessarily be evident at low strain levels as there is enough space in the gel to rearrange the fillers without destructive outcome. It should be emphasised that aggrecan, as previously discussed, is the main protein conferring compressive strength of native cartilage owing to its water binding capacity. Therefore, the very presence of collagen in a formulation is not expected to improve the compressive qualities of the gels.

The fact that Young's modulus is largely unaffected by the collagen is desirable as it is within the elastic range that the gel is intended to operate in practice, as this by definition should allow it to be subjected to many rounds of compression without compromising the mechanical properties. Importantly, according to the maximum elastic strain results, the LVR of all gel formulations encompasses the physiological deformations experienced during normal activities as discussed in section 2.1. It is possible that Young's modulus would be positively influenced at different pH and/or ionic strengths due to electrostatic interactions taking place between the alginate and collagen polymers. However, this is not of interest for applications with cells as these have strict requirements on the pH and ionic strengths of their environment. Noticeably, the highest reported Young's modulus for the formulations tested is still far below that reported for native articular cartilage. However, it should be considered that in an *in vivo* clinical application the gel would be supported by surrounding cartilage which would result in significantly higher elastic modulus owing to the improved retention of water as discussed in section 2.1.

The results from the stress relaxation trials demonstrates how the majority of the compressive strength for all gel formulations is attributed to the osmotic pressure provided by the water, demonstrating the similarities between hydrogels and articular cartilage with regards to their ability to retain water. as discussed in section 2.1. However, it should be noted that for in vivo applications the surrounding tissue would partially prevent water leakage, improving resistance against compression. The stress

relaxation times, which could influences cell behaviour as mentioned in section 2.2, where not consistently correlated with the concentrations of the gel components across different deformation levels. In the LVR, increasing the alginate appeared to reduce the stress relaxation times, i.e. make the gels more viscoelastic.

The heterogeneous distribution of fibrils in the pure collagen solutions observed by microscopy indicate a need of improving collagen fractionation, e.g. by mechanical separation, pre gelation to ensure a more homogenous spread throughout the alginate gel and possibly even allow for the formation of an IPN. The poor spread of the collagen network could also in part be a consequence of damaged telopeptides due to the pepsin digestion method chosen by the manufacturer for extracting and isolating the collagen, as discussed in section 4.8. Moreover, it is possible that the alginate gelation itself forces the collagen molecules together into aggregates which is reasonable given the manyfold stronger network created by the calcium induced alginate crosslinking. Additionally, issues with collagen aggregation could possibly be partially resolved by longer gelation times of the alginate, allowing more time for the collagen network to develop. However, this comes with its associated sets of challenges including preventing sedimentation and consequently heterogenous binding of the calcium ions and phase separation as a result of the slower gelation rate, resulting in weaker gels, as seen for the gels containing [redacted] Ca^{++}. Moreover, this presents a challenge in finding an optimal window for implementation of the cells to ensure the gels are enough liquid-like to prevent rupture post injection while having enough strength to maintain its structural integrity when subjected to a nutrient solution.

It is important to notice that the lack of positive influence from a large deformation standpoint does not render the collagen component redundant, as its main purpose in the system, as previously emphasised, is to serve as a biochemical cue and anchor point for the chondrocytes within the inert alginate matrix. Moreover, based on the trials of gelation kinetics, collagen contributes positively to the torsional elasticity of the gels which is an important attribute when integrating the cells to avoid cracks through which cell subsequently escape. However, it remains unknown whether the aggregation of the collagen influences the stiffness and length of the fibres formed, thereby reducing their bioactivity, as previously demonstrated and discussed in section 4.8.

In contrast, the findings suggests that inclusion of [redacted] in the alginate-collagen gels does not influence the mechanical properties on a macro level, which was its intended purpose. For pure collagen gels it provided a certain degree of mechanical strength as evident from the gelation kinetic trials but, as was evident from the Box-Behnken design results, the mechanical strength of the alginate-collagen gels is mainly dictated by the alginate crosslinking degree. However, it might still be the case that the [redacted] influence the mechanical properties on a micro scale by modulating the collagen fibres length and/or stiffness and could therefore impact cell behaviour and viability as discussed in section 4.8.

Cell studies were limited to focusing on finding ways of cell integration with minimal cell loss and high viability. Cell integration post gel formation was deemed necessary, as mixing of cells with gels pre gelation resulted in break up of the cell pellets into

small fragments, rendering the cells unviable. This further validated the theory that cells need to stay together in clusters to ensure viability in accordance with previous studies as described in section 1.2. Moreover, the gels with slow Ca^{++} release saw much greater cell retention, possibly due to the slower gelation rate and the early integration of cells in the hydrogel preventing ruptures from arising within the gel. The greater fractionation and cell spread seen for gels with collagen was possibly a result of too low gel firmness as reported in previous trials, indicating the need of either lowering the centrifugation speed or allowing gelation to occur for slightly longer pre cell integration to adjust for the collagens influence on the viscoelastic properties of the gel. It is possible that higher concentrations of collagen would be required to cause a significant positive impact on the mechanical properties of the gels. However, it is also important to balance the mechanical properties achieved against the concentrations required to achieve high bioactivity, as collagen concentration has been shown to influence fibre length and stiffness. Preliminary results from the cell studies suggests that the alginate-collagen gels break down faster compared to the pure alginate counterpart. Collagen might therefore act as a type of porogen which, if tweaked properly, could allow for easier remodelling by cells within the alginate network, thereby improving the rate of de novo cartilage formation. Moreover, the slightly weaker gels generated upon inclusion of collagen might improve nutrient and waste exchange with the surrounding media during cultivation.

It was concluded from the regression analysis that a substantial portion of the variance in the data is unexplained for. Possible explanations for the variance include the batch-to-batch variability of the alginate gels prepared due to the small amounts required to be weighed. An attempt was made to minimise this issue by preparing a large excess of gel in the magnitude of ten times the required volumes for each trial. Moreover, given the alginates polydispersity in molecular weight, there could still be variations introduced as a result of this. To reduce this issue, most of the gels with the same crosslinking degree were prepared from the same alginate gel batch. However, as discussed in section 2.2, the polydispersity of the alginate used in this study is considered to be low. Another source of variation was the challenge in achieving a consistent volumetric ratio when mixing the alginate and collagen gels due to the high viscosity of the solutions preventing accurate transfer of a given volume, although the error was controlled to be around 1 % at most. However, the main cause of the variations seen was likely the issues in creating gels with a consistent shape as air-bubbles were easily introduced when placing the lids on top of the gels in the molds. Therefore, the development of an improved mold system would likely be the most effective way to increase the consistency of the produced gels and the ability to distinguish between the performance of different formulations.

5.1 Future research

The unconfined compression trials conducted throughout this study are sufficient to fulfil the objective of distinguishing a difference in mechanical performance between the gel formulations. However, to more accurately predict the *in vivo* mechanical performance of the gels the use of a confined compression method is desirable since the characteristic mechanical features of hydrogels and cartilage alike stems from the

their ability to retain water, thereby creating osmotic pressure when situated in a confined environment as previously discussed in section 2.1.

By conducting compressional tests in a confined space using a textural analyser it is possible to more closely mimic the *in vivo* conditions, with surrounding articular cartilage providing support together with the synovial fluid that, similar to the fluid phase within the matrix, bears a portion of the load.

Moreover, the stress relaxation and fracture stress trials could be further complemented by cyclic loading trials were gels are repeatedly compressed in the LVR over extended periods of time to allow projections of the gels long term performance from a mechanical point of view, i.e. its wear resistance. Additionally, other attributes could be characterised including the Poisson ratio to further expand the understanding of the system's mechanical properties and how they can be affected.

The lack of lenses with sufficient magnification rendered the CLSM inoperable for this study and made it necessary to resort to a regular fluorescence microscope. CLSM would allow depth-profiling of the gels and could therefore provide more insights into the distribution of the gel components. A lens with appropriate magnification and resolution might also allow for quantitative measurements of the collagen aggregates size distribution in the different gel formulations. Moreover, it could be possible to observe the fibrillogenesis pattern by real-time imaging of the gel using confocal microscopy with a top plate incubator and fluorescent staining of the collagen fibres. This would provide more insights into the gelation kinetics registered by the time sweeps. Moreover, regarding the cell imaging, it would be of interest to complement the live/dead imaging with cell morphology and ECM staining as well as assay for chondrogenic markers to gain more insight into the state of the cells and how this is affected by varying the gel stiffness and porosity.

As previously discussed, it would be of interest to further investigate the impact of varying the Ca^{++} release rate, specifically to see whether slower gelation rates could possibly influence the development of the collagen network within the alginate gel. An alternative approach, which has previously been successful in creating an IPN of alginate and collagen, would be to mix the alginate with a collagen[redacted] mixture, adjusted pH to 7.4, allow the collagen network to develop at 37 °C and subsequently add the components inducing alginate gelation [46]. Investigating ways of improving collagen fractionation and dispersion pre gelation as well as comparing different collagen extraction methods is also of great interest as this might result in a more homogenous distribution of the network.

Additionally, the method of cell loading requires further development as indicated by the final trials. In particular, it would be of interest to investigate ways of achieving a more homogenous distribution of cells while ensuring large enough size of the aggregates to ensure high cell viability.

Lastly, it would be of interest to investigate the effect of choosing and combining other alginate sources with different MWs and G/M ratios with respect to their influence on the mechanical properties of the gels formed and its consequences on cell viability. Additionally, the effect on degradation rate of the matrix as well as the ECM produc-

tion would be of interest to study, since this has previously been documented to be influenced by these factors as discussed in sections 2.2 and 2.3.

6 Conclusions

The alginate and collagen components of the hydrogels formulated were not able to form an interpenetrating network within the parameter ranges investigated. This was indicated by the lack of a synergistic influence on the large deformation mechanical properties of the gels as evaluated by stress relaxation and unconfined compression. The lack of an interpenetrating network was further validated by microstructure analysis revealing aggregated clusters of collagen within the alginate network. Improved fractionating of the collagen pre gelation is possibly required to generate a more homogenous distribution of the network as indicated by the uneven spread of the network in the pure collagen gels. On the contrary, increasing collagen concentrations correlated negatively with the observed fracture stress and toughness of the gels but had no significant impact on Young's modulus. Moreover, the [redacted] [redacted] did not cause a positive impact on the large deformation mechanical properties. However, the combination of alginate, collagen and [redacted] did demonstrate a synergistic positive influence on the torsional elastic modulus as evaluated by time sweep. A successful method of loading the cells was established, as indicated by the viable cell clusters contained within the hydrogels as visualised by live/dead imaging. Moreover, cells showed high viability two weeks post loading demonstrating sufficient nutrient and gas exchange is occurring between the scaffold and the surrounding media.

References

1. Hunter D. J March L CM. Osteoarthritis in 2020 and beyond: a Lancet Commission. The lancet 2020 Nov; 396:1711–2. DOI: 10.1016/S0140-6736(20)32230-3
2. Mandelbaum BR and Mora SA. Cartilage Injury: Overview and Treatment Algorithm. *Articular Cartilage Lesions: A Practical Guide to Assessment and Treatment*. New York, NY: Springer New York, 2004. Chap. 188:35–46. DOI: 10.1007/978-0-387-21553-2_4
3. Kabir W, Di Bella C, Jo I, Gould D, and Choong PF. Human stem cell based tissue engineering for in vivo cartilage repair: a systematic review. Tissue Engineering Part B: Reviews 2021 Feb; 27:74–93. DOI: 10.1089/ten.TEB.2020.0155
4. Blair SN. Physical inactivity: the biggest public health problem of the 21st century. British journal of sports medicine 2009 Jan; 43:1–2
5. Prieto-Alhambra D, Hunter DJ, and Arden N. Osteoarthritis. 2nd ed. Vol. 6. 4617. Oxford University Press, 2014
6. CDC. Cost of Osteoarthritis. (accessed: 02.13.2022). Available from: https://www.cdc.gov/arthritis/data_statistics/cost.htm
7. Kwon H, Brown WE, Lee CA, Wang D, Paschos N, Hu JC, and Athanasiou KA. Surgical and tissue engineering strategies for articular cartilage and meniscus repair. Nature Reviews Rheumatology 2019 Sep; 15:550–70. DOI: 10.1038/s41584-019-0255-1
8. Fox A, Bedi A, and Rodeo S. The Basic Science of Articular Cartilage: Structure, Composition, and Function. Sports health 2009 Nov; 1:461–8. DOI: 10.1177/1941738109350438
9. Yang X, Lu Z, Wu H, Li W, Zheng L, and Zhao J. Collagen-alginate as bioink for three-dimensional (3D) cell printing based cartilage tissue engineering. Materials Science and Engineering: C 2018 Feb; 83:195–201. DOI: 10.1016/j.msec.2017.09.002
10. Zhang L, Hu J, and Athanasiou KA. The role of tissue engineering in articular cartilage repair and regeneration. Critical Reviews™ in Biomedical Engineering 2009 Jul; 37:1–57. DOI: 10.1615/critrevbiomedeng.v37.i1-2.10
11. Evenbratt H, Andreasson L, Bicknell V, Brittberg M, Mobini R, and Simonsson S. Insights into the present and future of cartilage regeneration and joint repair. Cell Regeneration 2022 Feb; 11:1–16. DOI: 10.1186/s13619-021-00104-5
12. Zhang W, Ouyang H, Dass CR, and Xu J. Current research on pharmacologic and regenerative therapies for osteoarthritis. Bone research 2016 Mar; 4:1–14. DOI: 10.1038/boneres.2015.40
13. Yang F, Zhao J, Koshut WJ, Watt J, Riboh JC, Gall K, and Wiley BJ. A synthetic hydrogel composite with the mechanical behavior and durability of cartilage. Advanced Functional Materials 2020 Jun; 30:2003451. DOI: 10.1002/adfm.202003451

14. Jin GZ and Kim HW. Efficacy of collagen and alginate hydrogels for the prevention of rat chondrocyte dedifferentiation. Journal of tissue engineering 2018 Oct; 9:2041731418802438. DOI: 10.1177/2041731418802438

15. Andreasson L, Evenbratt H, Mobini R, and Simonsson S. Differentiation of induced pluripotent stem cells into definitive endoderm on Activin A-functionalized gradient surfaces. Journal of Biotechnology 2021 Nov; 325:173–8. DOI: 10.1016/j.jbiotec.2020.10.030

16. Kim SH, Jung YM, and Kim SH. Cell aggregate-hydrogel-polymer scaffold complex for cartilage regeneration, method for the preparation thereof and composition comprising the same. US Patent App. 12/614,561. 2010 May

17. Schwarz S, Kuth S, Distler T, Gögele C, Stölzel K, Detsch R, Boccaccini AR, and Schulze-Tanzil G. 3D printing and characterization of human nasoseptal chondrocytes laden dual crosslinked oxidized alginate-gelatin hydrogels for cartilage repair approaches. Materials Science and Engineering: C 2020 Nov; 116:111189. DOI: 10.1016/j.msec.2020.111189

18. Vázquez-Portalatın N, Kilmer CE, Panitch A, and Liu JC. Characterization of collagen type I and II blended hydrogels for articular cartilage tissue engineering. Biomacromolecules 2016 Oct; 17:3145–52. DOI: 10.1021/acs.biomac.6b00684

19. Mansour JM. Biomechanics of cartilage. Vol. 2. Lippincott Williams and Wilkins: Philadelphia, PA, 2003 :66–79

20. Ledo AM, Vining KH, Alonso MJ, Garcia-Fuentes M, and Mooney DJ. Extracellular matrix mechanics regulate transfection and SOX9-directed differentiation of mesenchymal stem cells. Acta biomaterialia 2020 Jul; 110:153–63. DOI: 10.1016/j.actbio.2020.04.027

21. Candiello J, Singh SS, Task K, Kumta PN, and Banerjee I. Early differentiation patterning of mouse embryonic stem cells in response to variations in alginate substrate stiffness. Journal of biological engineering 2013 Apr; 7:1–14. DOI: 10.1186/1754-1611-7-9

22. He B, Wu J, Chim SM, Xu J, and Kirk TB. Microstructural analysis of collagen and elastin fibres in the kangaroo articular cartilage reveals a structural divergence depending on its local mechanical environment. Osteoarthritis and cartilage 2013 Jan; 21:237–45. DOI: 10.1016/j.joca.2012.10.008

23. Fortin M, Soulhat J, Shirazi-Adl A, Hunziker E, and Buschmann M. Unconfined compression of articular cartilage: nonlinear behavior and comparison with a fibril-reinforced biphasic model. J. Biomech. Eng. 2000 Apr; 122:189–95. DOI: 10.1115/1.429641

24. Kabir W, Di Bella C, Choong PF, and O'Connell CD. Assessment of native human articular cartilage: a biomechanical protocol. Cartilage 2021; 13:427S–437S

25. Möller T, Amoroso M, Hägg D, Brantsing C, Rotter N, Apelgren P, Lindahl A, Kölby L, and Gatenholm P. In vivo chondrogenesis in 3D bioprinted human cell-laden hydrogel constructs. Plastic and reconstructive surgery global open 2017 Feb; 5:e1227. DOI: 10.1097/GOX.0000000000001227

26. Kilmer CE, Battistoni CM, Cox A, Breur GJ, Panitch A, and Liu JC. Collagen type I and II blend hydrogel with autologous mesenchymal stem cells as a scaffold for articular cartilage defect repair. ACS biomaterials science & engineering 2020 Jun; 6:3464–76. DOI: 10.1021/acsbiomaterials.9b01939

27. Lee KY and Mooney DJ. Alginate: properties and biomedical applications. Progress in polymer science 2012 Jan; 37:106–26. DOI: 10.1016/j.progpolymsci.2011.06.003

28. Hu T and Lo AC. Collagen–Alginate Composite Hydrogel: Application in Tissue Engineering and Biomedical Sciences. Polymers 2021 Jun; 13:1852. DOI: 10.3390/polym13111852

29. Shojarazavi N, Mashayekhan S, Pazooki H, Mohsenifard S, and Baniasadi H. Alginate/cartilage extracellular matrix-based injectable interpenetrating polymer network hydrogel for cartilage tissue engineering. Journal of Biomaterials Applications 2021 Jun; 36:803–17. DOI: 10.1177/08853282211024020

30. Mitrousis N, Fokina A, and Shoichet MS. Biomaterials for cell transplantation. Nature Reviews Materials 2018 Oct; 3:441–56. DOI: 10.1038/s41578-018-0057-0

31. Farrés IF and Norton I. Formation kinetics and rheology of alginate fluid gels produced by in-situ calcium release. Food Hydrocolloids 2014 Oct; 40:76–84. DOI: 10.1016/j.foodhyd.2014.02.005

32. Liu G, Zhou H, Wu H, Chen R, and Guo S. Preparation of alginate hydrogels through solution extrusion and the release behavior of different drugs. Journal of Biomaterials science, Polymer edition 2016 Dec; 27:1808–23. DOI: 10.1080/09205063.2016.1237452

33. Zhang J, Daubert CR, and Foegeding EA. Fracture analysis of alginate gels. Journal of food science 2005; 70:e425–e431. DOI: 10.1111/j.1365-2621.2005.tb11471.x

34. Phillips GO and Williams PA. Handbook of hydrocolloids. Elsevier, 2009

35. Elosegui-Artola A, Gupta A, Najibi AJ, Seo BR, Garry R, Tringides CM, Lázaro I de, Darnell M, Gu W, Zhou Q, et al. Matrix viscoelasticity controls spatiotemporal tissue organization. Nature Materials 2023 Dec; 22:117–27. DOI: 10.1038/s41563-022-01400-4

36. Neves MI, Moroni L, and Barrias CC. Modulating alginate hydrogels for improved biological performance as cellular 3D microenvironments. Frontiers in bioengineering and biotechnology 2020; 8:665. DOI: 10.3389/fbioe.2020.00665

37. Ström AHE. Characterisation of pectin fine-structure and its effect on supramolecular properties. PhD thesis. NUI, 2006

38. Ameer GA and Langer Jr RS. Mesh-gel constructs for cell delivery containing enzymes and/or enzyme inhibitors to control gel degradation. US Patent 6,699,470. 2004 Mar

39. Yamamoto K, Yuguchi Y, Stokke BT, Sikorski P, and Bassett DC. Local structure of Ca2+ alginate hydrogels gelled via competitive ligand exchange and measured by small angle X-ray scattering. Gels 2019 Jan; 5:3. DOI: 10.3390/gels5010003

40. Augst AD, Kong HJ, and Mooney DJ. Alginate hydrogels as biomaterials. Macromolecular bioscience 2006 Aug; 6:623–33. DOI: 10.1002/mabi.200600069

41. Kuo CK and Ma PX. Maintaining dimensions and mechanical properties of ionically crosslinked alginate hydrogel scaffolds in vitro. Journal of Biomedical Materials Research Part A: An Official Journal of The Society for Biomaterials, The Japanese Society for Biomaterials, and The Australian Society for Biomaterials and the Korean Society for Biomaterials 2008 Mar; 84:899–907. DOI: 10.1002/jbm.a.31375

42. Huebsch ND, Madl CM, Lee K, Xu MM, and Mooney DJ. Injectable, pore-forming hydrogels for materials-based cell therapies. US Patent App. 17/522,297. 2022 Jun

43. Drury JL, Boontheekul T, and Mooney DJ. Cellular cross-linking of peptide modified hydrogels. Journal of biomechanical engineering 2005 Apr; 127:220–8. DOI: 10.1115/1.1865194

44. Athanasiou KA, Darling EM, and Hu JC. Articular cartilage tissue engineering. Vol. 1. 1. Morgan & Claypool Publishers, 2009 :1–182

45. Walimbe T and Panitch A. Best of both hydrogel worlds: Harnessing bioactivity and tunability by incorporating glycosaminoglycans in collagen hydrogels. Bioengineering 2020 Dec; 7:156. DOI: 10.3390/bioengineering7040156

46. Cunha CB da, Klumpers DD, Li WA, Koshy ST, Weaver JC, Chaudhuri O, Granja PL, and Mooney DJ. Influence of the stiffness of three-dimensional alginate / collagen-I interpenetrating networks on fibroblast biology. Biomaterials 2014 Oct; 35:8927–36. DOI: 10.1016/j.biomaterials.2014.06.047

47. Baniasadi M and Minary-Jolandan M. Alginate-collagen fibril composite hydrogel. Materials 2015 Feb; 8:799–814. DOI: 10.3390/ma8020799

48. Connelly JT, Garcıa AJ, and Levenston ME. Inhibition of in vitro chondrogenesis in RGD-modified three-dimensional alginate gels. Biomaterials 2007 Nov; 28:1071–83. DOI: 10.1016/j.biomaterials.2006.10.006

49. Xie J, Bao M, Bruekers SM, and Huck WT. Collagen gels with different fibrillar microarchitectures elicit different cellular responses. ACS applied materials & interfaces 2017 Jun; 9:19630–7. DOI: 10.1021/acsami.7b03883

50. Gelse K, Pöschl E, and Aigner T. Collagens—structure, function, and biosynthesis. Advanced drug delivery reviews 2003 Nov; 55:1531–46. DOI: 10.1016/j.addr.2003.08.002

51. Shannon G, Novak T, Mousoulis C, Voytik-Harbin S, and Neu C. Temperature and concentration dependent fibrillogenesis for improved magnetic alignment of collagen gels. Rsc Advances 2015 Nov; 5:2113–21. DOI: 10.1039/C4RA11480A

52. Antipova O and Orgel JP. In situ D-periodic molecular structure of type II collagen. Journal of Biological Chemistry 2010 Jan; 285:7087–96. DOI: 10.1074/jbc.M109.060400

53. Kadler KE, Holmes DF, Trotter JA, and Chapman JA. Collagen fibril formation. Biochemical Journal 1996 May; 316:1–11. DOI: 10.1042/bj3160001

54. Yang C, Hillas PJ, Báez JA, Nokelainen M, Balan J, Tang J, Spiro R, and Polarek JW. The application of recombinant human collagen in tissue engineering. BioDrugs 2004 Aug; 18:103–19. DOI: 10.2165/00063030-200418020-00004

55. Kreger S, Bell B, Bailey J, Stites E, Kuske J, Waisner B, and Voytik-Harbin S. Polymerization and matrix physical properties as important design considerations for soluble collagen formulations. Biopolymers: Original Research on Biomolecules 2010 Aug; 93:690–707. DOI: 10.1002/bip.21431

56. Waheed A, Rao KS, and Gupta P. Mechanism of dye binding in the protein assay using eosin dyes. Analytical biochemistry 2000 Dec; 287:73–9. DOI: 10.1006/abio.2000.4793

57. Hayashi T and NAGAI Y. Effect of pH on the stability of collagen molecule in solution. The Journal of Biochemistry 1973 May; 73:999–1006. DOI: 10.1093/oxfordjournals.jbchem.a130184

58. abcam. Anti-Collagen I antibody (ab34710). Available from: https://www.abcam.com/products/primary-antibodies/collagen-i-antibody-ab34710.html

59. Sigma-Aldrich. LIVE/DEAD™ Viability/Cytotoxicity Kit, for mammalian cells. Available from: https://www.thermofisher.com/order/catalog/product/L3224

60. Silva MP, Badruddin IJ, Tonon T, Rahatekar S, and Gomez LD. Environmentally benign alginate extraction and fibres spinning from different European Brown algae species. International journal of biological macromolecules 2023 Jan; 226:434–42. DOI: 10.1016/j.ijbiomac.2022.11.306

61. Nguyen NK, Borkowski JJ, and Vuong MP. Perspective Chapter: Cyclic Generation of Box-Behnken Designs and New Second-Order Designs. 2022 Oct. DOI: 10.5772/intechopen.107178

62. Karmoker JR, Hasan I, Ahmed N, Saifuddin M, and Reza MS. Development and optimization of acyclovir loaded mucoadhesive microspheres by box–Behnken design. Dhaka University Journal of Pharmaceutical Sciences 2019 Apr; 18:1–12. DOI: 10.3329/dujps.v18i1.41421

63. Ferreira SC, Bruns R, Ferreira HS, Matos GD, David J, Brandão G, Silva EP da, Portugal L, Dos Reis P, Souza A, et al. Box-Behnken design: An alternative for the optimization of analytical methods. Analytica chimica acta 2007 Aug; 597:179–86. DOI: 10.1016/j.aca.2007.07.011

Appendices

A Alginate SEC data

In figure S1 the data on alginate Manugel DMB generated by size exclusion chromatography (SEC) is presented.

	Mn (kDa)	Uncertainty	Mp (kDa)	Uncertainty	Mw (kDa)	Uncertainty	Polydispersity (Mw/Mn)	Uncertainty	rz (nm)	Uncertainty	rh(v)z (nm)	Uncertainty	Mass recovery (%)	[η]z (mL/g)	Uncertainty
Alginat(001)	121.0	0.4%	117.6	0.3%	161.3	0.5%	1.332	0.672%	86.0	0.5%	41.0	0.2%	65.6	1869.610	0.089%
Alginat(002)	125.2	0.3%	116.9	0.3%	172.4	0.5%	1.378	0.649%	91.5	0.5%	42.9	0.2%	67.0	1874.965	0.131%
Alginat(003)	128.1	0.4%	118.3	0.3%	183.4	0.6%	1.432	0.782%	97.5	0.5%	45.9	0.3%	66.8	1971.480	0.102%
Average	124.8		117.6		172.4		1.381		91.7		43.3		66.5	1905.352	
Standard deviation	3.5		0.7		11.1		0.050		5.8		2.5		0.7	57.331	
% Standard deviation	2.8		0.6		6.4		3.618		6.3		5.7		1.1	3.009	
Minimum	121.0		116.9		161.3		1.332		86.0		41.0		65.6	1869.610	
Maximum	128.1		118.3		183.4		1.432		97.5		45.9		67.0	1971.480	

Figure S1: Manugel DMB alginate data obtained by SEC.

B Alg-Col gels with rapid Ca^{++} release - Frequency sweeps

In figure S2 and S3 the resulting storage and loss modulus during frequency sweep measurements of the gels are presented.

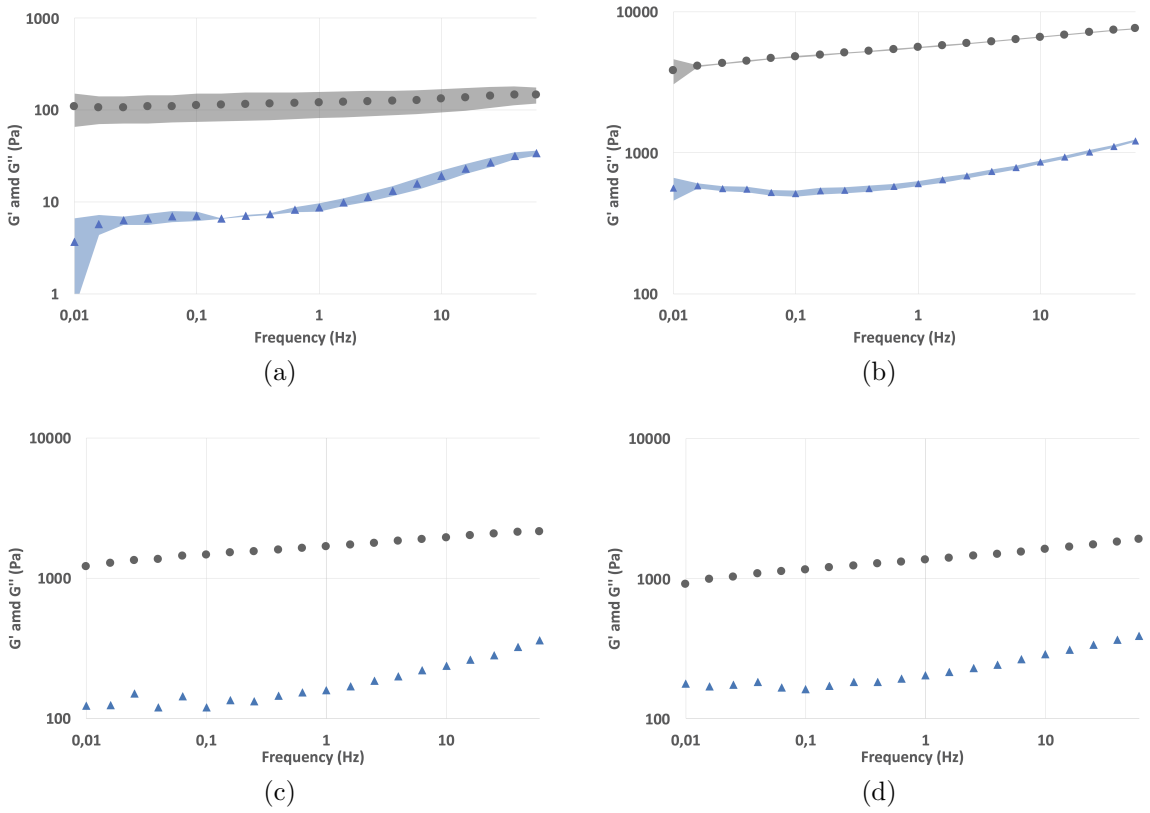

Figure S2: Frequency sweeps of Alg-Col gels: (a) Alg-Col-[redacted]; (b) Alg-Col-[redacted]; (c) Alg-Col-[redacted] and (d) Alg-Col-[redacted]. Grey dots and light blue triangles symbolise the storage modulus and the loss modulus respectively. The coloured area around the datapoints represents the standard deviation of the modulus.

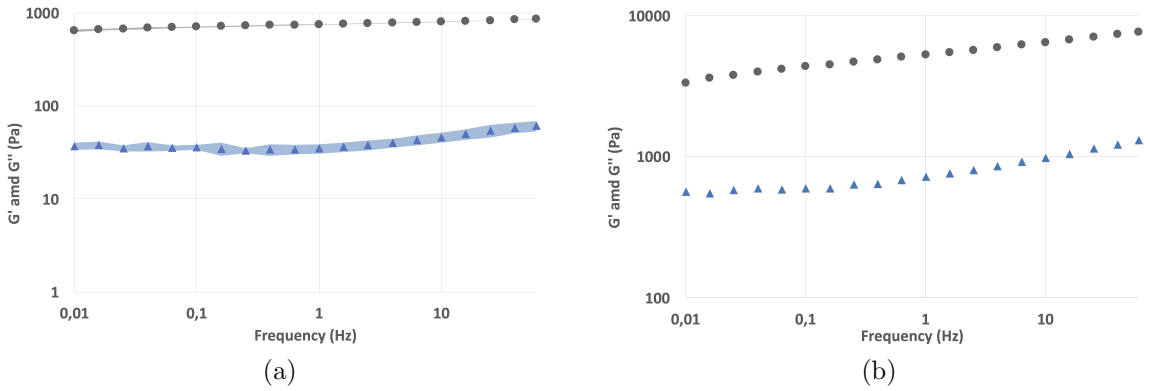

Figure S3: Frequency sweeps of Alg-Col gels: (a) Alg-Col-[redacted] and (b) Alg-Col-[redacted]. Grey dots and light blue triangles symbolise the storage modulus and the loss modulus respectively. The coloured area around the datapoints represents the standard deviation of the modulus.

C Regression models of Alg-Col gels with slow Ca^{++} release

Find below complete and reduced regression models including their fit, as defined by R^2 values, as well as the coded coefficients of the parameters and their significance level, as defined by their P-value.

C.1 Fracture stress models

Model Summary

S	R-sq	R-sq(adj)	R-sq(pred)
7,67196	87,08%	82,77%	76,79%

Coded Coefficients

Term	Coef	SE Coef	T-Value	P-Value	VIF
Constant	19,33	5,42	3,56	0,001	
Alg	15,86	1,61	9,86	0,000	1,01
Col	-9,01	1,61	-5,60	0,000	1,01
[redacted]	-0,85	1,57	-0,55	0,590	1,00
Alg*Alg	14,43	3,34	4,32	0,000	1,65
Col*Col	11,90	3,34	3,56	0,001	1,65
[redacted]	17,85	3,34	5,34	0,000	1,60
Alg*Col	-5,73	2,33	-2,46	0,021	1,02
Alg*[redacted]	-3,12	2,21	-1,41	0,171	1,00
Col*[redacted]	-5,32	2,21	-2,40	0,023	1,00

(a)

Model Summary

S	R-sq	R-sq(adj)	R-sq(pred)
7,70849	85,99%	82,61%	79,96%

Coded Coefficients

Term	Coef	SE Coef	T-Value	P-Value	VIF
Constant	19,33	5,45	3,55	0,001	
Alg	15,86	1,62	9,81	0,000	1,01
Col	-9,01	1,62	-5,57	0,000	1,01
Alg*Alg	14,43	3,36	4,30	0,000	1,65
Col*Col	11,90	3,36	3,54	0,001	1,65
[redacted]	17,85	3,36	5,32	0,000	1,60
Alg*Col	-5,73	2,35	-2,44	0,021	1,02
Col*[redacted]	-5,32	2,23	-2,39	0,023	1,00

(b)

Figure S4: Regression model of fracture stress: (a) Quadratic and (b) Reduced model (Stepwise elimination)

C.2 Models of fracture strain

Model Summary

S	R-sq	R-sq(adj)	R-sq(pred)
0,0155456	75,24%	66,99%	53,24%

Coded Coefficients

Term	Coef	SE Coef	T-Value	P-Value	VIF
Constant	0,5450	0,0110	49,58	0,000	
Alg	-0,01181	0,00326	-3,62	0,001	1,01
Col	-0,01764	0,00326	-5,41	0,000	1,01
[redacted]	0,00250	0,00317	0,79	0,438	1,00
Alg*Alg	0,00444	0,00677	0,66	0,517	1,65
Col*Col	0,03111	0,00677	4,59	0,000	1,65
[redacted]	0,01972	0,00677	2,91	0,007	1,60
Alg*Col	-0,01444	0,00473	-3,05	0,005	1,02
Alg*[redacted]	0,00083	0,00449	0,19	0,854	1,00
Col*[redacted]	0,01083	0,00449	2,41	0,023	1,00

(a)

Model Summary

S	R-sq	R-sq(adj)	R-sq(pred)
0,0150415	74,25%	69,10%	58,41%

Coded Coefficients

Term	Coef	SE Coef	T-Value	P-Value	VIF
Constant	0,55085	0,00622	88,63	0,000	
Alg	-0,01186	0,00315	-3,76	0,001	1,01
Col	-0,01769	0,00315	-5,61	0,000	1,01
Col*Col	0,02862	0,00542	5,28	0,000	1,13
[redacted]	0,01734	0,00553	3,14	0,004	1,14
Alg*Col	-0,01455	0,00457	-3,18	0,003	1,01
Col*[redacted]	0,01083	0,00434	2,49	0,018	1,00

(b)

Figure S5: Regression models of fracture strain: (a) Quadratic and (b) Reduced model (Stepwise elimination)

C.3 Models of toughness

Model Summary

S	R-sq	R-sq(adj)	R-sq(pred)
0,911862	89,23%	85,64%	80,45%

Coded Coefficients

Term	Coef	SE Coef	T-Value	P-Value	VIF
Constant	3,390	0,645	5,26	0,000	
Alg	2,038	0,191	10,65	0,000	1,01
Col	-1,342	0,191	-7,02	0,000	1,01
[redacted]	-0,070	0,186	-0,38	0,708	1,00
Alg*Alg	2,053	0,397	5,17	0,000	1,65
Col*Col	1,974	0,397	4,97	0,000	1,65
[redacted]	2,276	0,397	5,73	0,000	1,60
Alg*Col	-0,802	0,277	-2,89	0,007	1,02
Alg*[redacted]	-0,139	0,263	-0,53	0,601	1,00
Col*[redacted]	-0,295	0,263	-1,12	0,272	1,00

(a)

Model Summary

S	R-sq	R-sq(adj)	R-sq(pred)
0,891553	88,56%	86,27%	83,87%

Coded Coefficients

Term	Coef	SE Coef	T-Value	P-Value	VIF
Constant	3,390	0,630	5,38	0,000	
Alg	2,038	0,187	10,90	0,000	1,01
Col	-1,342	0,187	-7,18	0,000	1,01
Alg*Alg	2,053	0,388	5,29	0,000	1,65
Col*Col	1,974	0,388	5,08	0,000	1,65
[redacted]	2,276	0,388	5,86	0,000	1,60
Alg*Col	-0,802	0,271	-2,96	0,006	1,02

(b)

Figure S6: Regression model of toughness: (a) Quadratic and (b) Reduced model (Stepwise elimination)

C.4 Models of Young's modulus

Model Summary

S	R-sq	R-sq(adj)	R-sq(pred)
2,50965	40,44%	20,59%	0,00%

Coded Coefficients

Term	Coef	SE Coef	T-Value	P-Value	VIF
Constant	15,86	1,77	8,93	0,000	
Alg	1,992	0,526	3,78	0,001	1,01
Col	-0,077	0,526	-0,15	0,885	1,01
[redacted]	-0,517	0,512	-1,01	0,322	1,00
Alg*Alg	1,70	1,09	1,55	0,132	1,65
Col*Col	0,80	1,09	0,73	0,469	1,65
[redacted]	0,17	1,09	0,16	0,877	1,60
Alg*Col	0,151	0,764	0,20	0,845	1,02
Alg*[redacted]	0,374	0,724	0,52	0,610	1,00
Col*[redacted]	0,078	0,724	0,11	0,915	1,00

(a)

Model Summary

S	R-sq	R-sq(adj)	R-sq(pred)
2,37842	30,66%	28,68%	21,73%

Coded Coefficients

Term	Coef	SE Coef	T-Value	P-Value	VIF
Constant	17,518	0,391	44,78	0,000	
Alg	1,952	0,496	3,93	0,000	1,00

(b)

Figure S7: Regression model of Young's modulus: (a) Quadratic and (b) Reduced model (Stepwise elimination)

C.5 Models of maximum elastic strain

Model Summary

S	R-sq	R-sq(adj)	R-sq(pred)
0,0120281	73,75%	65,00%	48,68%

Term	Coef	SE Coef	T-Value	P-Value	VIF
Constant	0,25000	0,00851	29,39	0,000	
Alg	-0,01854	0,00252	-7,35	0,000	1,01
Col	-0,00062	0,00252	-0,25	0,806	1,01
[redacted]	0,00125	0,00246	0,51	0,615	1,00
Alg*Alg	-0,02104	0,00524	-4,02	0,000	1,65
Col*Col	-0,01521	0,00524	-2,90	0,007	1,65
[redacted]	-0,01646	0,00524	-3,14	0,004	1,60
Alg*Col	-0,00958	0,00366	-2,62	0,014	1,02
Alg*[redacted]	0,00083	0,00347	0,24	0,812	1,00
Col*[redacted]	0,00167	0,00347	0,48	0,635	1,00

(a)

Model Summary

S	R-sq	R-sq(adj)	R-sq(pred)
0,0113511	73,16%	68,83%	60,11%

Coded Coefficients

Term	Coef	SE Coef	T-Value	P-Value	VIF
Constant	0,25000	0,00803	31,15	0,000	
Alg	-0,01851	0,00238	-7,79	0,000	1,01
Alg*Alg	-0,02101	0,00494	-4,25	0,000	1,65
Col*Col	-0,01518	0,00494	-3,07	0,004	1,65
[redacted]	-0,01649	0,00494	-3,34	0,002	1,60
Alg*Col	-0,00952	0,00344	-2,76	0,010	1,01

(b)

Figure S8: Regression models of maximum elastic strain: (a) Quadratic and (b) Reduced model (Stepwise elimination)

C.6 Models of initial stress pre relaxation

Model Summary

S	R-sq	R-sq(adj)	R-sq(pred)
2,47992	85,10%	80,33%	72,95%

Coded Coefficients

Term	Coef	SE Coef	T-Value	P-Value	VIF
Constant	16,99	1,06	16,02	0,000	
Alg	6,116	0,547	11,18	0,000	1,02
Col	0,942	0,547	1,72	0,097	1,02
[redacted]	0,116	0,535	0,22	0,830	1,02
Col*Col	1,673	0,932	1,80	0,085	1,13
[redacted]	-1,897	0,954	-1,99	0,058	1,15
Alg*Col	1,048	0,798	1,31	0,201	1,02
Alg*[redacted]	0,757	0,755	1,00	0,325	1,02
Col*[redacted]	-1,740	0,755	-2,31	0,030	1,02

(a)

Model Summary

S	R-sq	R-sq(adj)	R-sq(pred)
2,75605	77,17%	75,70%	73,17%

Coded Coefficients

Term	Coef	SE Coef	T-Value	P-Value	VIF
Constant	18,211	0,796	22,89	0,000	
Alg	6,023	0,602	10,00	0,000	1,00
[redacted]	-2,422	0,989	-2,45	0,020	1,00

(b)

Figure S9: Regression model of initial stress pre relaxation at 49 % deformation: (a) Quadratic and (b) Reduced model (Stepwise elimination)

C.7 Models of stress post relaxation

Model Summary

S	R-sq	R-sq(adj)	R-sq(pred)
0,678370	89,31%	85,30%	79,49%

Coded Coefficients

Term	Coef	SE Coef	T-Value	P-Value	VIF
Constant	1,170	0,480	2,44	0,022	
Alg	1,755	0,150	11,73	0,000	1,02
Col	-0,361	0,150	-2,41	0,024	1,02
[redacted]	0,581	0,146	3,97	0,001	1,02
Alg*Alg	0,806	0,301	2,68	0,013	1,58
Col*Col	0,670	0,301	2,23	0,036	1,58
[redacted]	0,182	0,302	0,60	0,552	1,53
Alg*Col	-0,447	0,219	-2,04	0,052	1,03
Alg*[redacted]	0,337	0,207	1,63	0,116	1,02
Col*[redacted]	-0,759	0,207	-3,68	0,001	1,02

(a)

Model Summary

S	R-sq	R-sq(adj)	R-sq(pred)
0,726613	86,20%	83,13%	77,97%

Coded Coefficients

Term	Coef	SE Coef	T-Value	P-Value	VIF
Constant	1,322	0,310	4,27	0,000	
Alg	1,774	0,160	11,11	0,000	1,01
Col	-0,362	0,160	-2,26	0,032	1,02
[redacted]	0,602	0,156	3,85	0,001	1,01
Alg*Alg	0,774	0,277	2,80	0,009	1,17
Col*Col	0,670	0,276	2,42	0,022	1,16
Col*[redacted]	-0,754	0,221	-3,41	0,002	1,02

(b)

Figure S10: Regression models of stress post relaxation at 49 % deformation: (a) Quadratic and (b) Reduced model (Stepwise elimination)

C.8 Models of percent of initial stress post relaxation

Model Summary

S	R-sq	R-sq(adj)	R-sq(pred)
5,75271	66,23%	53,56%	36,21%

Coded Coefficients

Term	Coef	SE Coef	T-Value	P-Value	VIF
Constant	6,96	4,07	1,71	0,100	
Alg	6,02	1,27	4,74	0,000	1,02
Col	-2,24	1,27	-1,76	0,091	1,02
[redacted]	3,26	1,24	2,63	0,015	1,02
Alg*Alg	2,17	2,55	0,85	0,404	1,58
Col*Col	2,89	2,55	1,13	0,269	1,58
[redacted]	2,99	2,56	1,17	0,253	1,53
Alg*Col	-3,27	1,86	-1,76	0,091	1,03
Alg*[redacted]	0,74	1,75	0,42	0,675	1,02
Col*[redacted]	-4,54	1,75	-2,59	0,016	1,02

(a)

Model Summary

S	R-sq	R-sq(adj)	R-sq(pred)
5,97653	54,44%	49,88%	39,85%

Coded Coefficients

Term	Coef	SE Coef	T-Value	P-Value	VIF
Constant	12,26	1,03	11,90	0,000	
Alg	6,26	1,31	4,79	0,000	1,00
[redacted]	3,22	1,28	2,51	0,018	1,01
Col*[redacted]	-4,69	1,81	-2,59	0,015	1,00

(b)

Figure S11: Regression model of stress post relaxation relative to initial stress at 49 % deformation: (a) Quadratic and (b) Reduced model (Stepwise elimination)

DEPARTMENT OF CHEMISTRY AND CHEMICAL ENGINEERING
OLIVER FORSELL - CHALMERS UNIVERSITY OF TECHNOLOGY

HYDROGELS AS SCAFFOLDS FOR STEM CELL THERAPY WITH FOCUS ON CARTILAGE

Gothenburg, Sweden 2023
www.chalmers.se

CHALMERS
UNIVERSITY OF TECHNOLOGY